ACS OMEGA

http://pubs.acs.org/journal/acsodf

Mini-Review

Strategies to Design Single-Molecule Toroics Using Triangular $\{Ln_3\}_n$ Motifs

Kuduva R. Vignesh* and Gopalan Rajaraman*

Cite This: *ACS Omega* 2021, 6, 32349−32364

Read Online

ACCESS | Metrics & More | Article Recommendations

ABSTRACT: In this mini-review, we highlight the research advanced in the field of single-molecule toroics (SMTs) with a specific focus on the triangular Ln_3-based SMTs. SMTs are molecules with a toroidal magnetic state and are insensitive to homogeneous magnetic fields but cooperate with charge and spin currents. The rapid growth in the area of SMTs witnessed in recent years is correlated not only to the interest to understand the fundamental physics of these molecules but also to the intriguing potential applications proposed, as the SMTs have several advantages compared to other classes of molecules such as single-molecule magnets (SMMs). The important chemico-structural strategy in SMT chemistry is to choose and design ligand and bridging species that will help to attain toroidal behavior. Considering this primarily, all the Dy_3 SMTs reported so far are summarized, showing how utilizing different peripheral ligands influences the toroidal nature beyond the role of the symmetry of the molecule and stronger dipolar interactions. Likewise, linking Dy_3 toroidal units through 3d ions with suitable peripheral/bridging ligands enhances the toroidal magnetic moment and leads to fascinating physics of ferrotoroidal/antiferrotoridal behavior. Further, we have also summarized the recently reported non-Dy triangular SMTs.

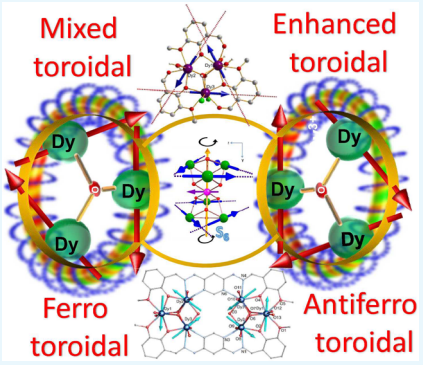

INTRODUCTION

Single-molecule toroics (SMTs) are bistable molecules similar to single-molecule magnets (SMMs) but with a toroidal magnetic state. The noncollinear arrangement of the magnetic moments of each metal center in SMTs can lead to interesting magnetic behavior.[1−12] SMTs have possible wide-ranging applications in quantum computing, memory storage, and spintronics devices and the development of magneto−electric coupling for multiferroic materials.[13−15] Noteworthily, the magnetic field produced by toroidal moments decays more rapidly than the field produced by a magnetic dipole; thus, the memory storage devices or qubits designed utilizing toroidal moments will be more densely packed than SMMs or spin qubits, respectively.[3] For a molecule to show SMT behavior, it should possess the following criteria: (a) high molecular symmetry, (b) local magnetic moment, and (c) strong intramolecular magnetic interactions.[11,12] Both experiments and theory have played a vital role in detecting the presence of toroidal magnetic moments. Particularly *ab initio* calculations based on the CASSCF/RASSI-SO method offered significant insights into the SMT behavior.[11,12] Usually, SMT complexes display a stepped hysteresis profile and a pronounced S-shaped curve in the magnetization isotherm plots at low fields and low temperatures; however, these profiles are not witnessed in some cases.[1−12] Additionally, single-crystal magnetic studies, EPR, and Torque magnetometry offer clues on the SMT molecules,[11] though unambiguous confirmation requires accurate spectral methods such as NMR, which can probe the magnetic dynamics of individual Ln(III) ions via line broadening.[16,17]

There are different shaped SMTs with numerous examples of Dy_3 triangles,[1−5,9] planar/cubic Dy_4,[18,19] wheel Dy_6,[17,20] a snub-square Dy_8,[21] and double Dy_3 + Dy_3 triangles.[6,7,22,23] Toroidal moments are reported for dysprosium (Dy^{III}) complexes; however, recently we reported the SMTs possessing Tb^{III} and Ho^{III} ions as well.[20,24] SMTs have been reported by connecting two molecular triangles, for example, via a 3d ion, and such systems offer a chance to observe properties such as ferrotoroidicity in 3d−4f-based complexes,[25] which in turn is of interest for the strategy of molecule-based multiferroics with a magneto−electric coupling.[13−15] A con-rotating ferrotoroidal ground-state behavior in a series of heptanuclear $\{CrLn_6\}$ complexes (Ln = Dy, Tb, Ho) has been observed by us.[24,25] The ferrotoroidal moments were recently observed in another large $\{Fe_{18}Dy_6\}$ cluster where two molecular Dy_3 triangles are connected by a $\{Fe_{18}\}$ ring.[26] Though several SMTs have been reported to date, the most seen archetype system is the triangular Dy_3 motif (Figure 1). Therefore, here we represented

Received: September 24, 2021
Accepted: November 12, 2021
Published: November 29, 2021

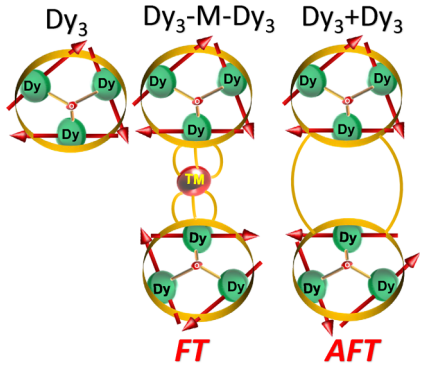

Figure 1. Schematic representation of a different type of triangular SMTs discussed here. Red arrows are Dy(III) local g_z magnetization axes. Middle and right pictures are representing ferrotoroidal (FT) and antiferrotoroidal (AFT) behavior.[24,25]

mainly the triangle-shaped SMTs and classified them based on their peripheral ligands. Moreover, how toroidicity is enhanced by connecting two Dy_3 triangles through bridging ligands or via a 3d ion and the other lanthanide-based Ln_3 triangular SMTs is also discussed in this mini-review, using representative examples (see Table 1).

COMPARING DY_3 SMTS BY PERIPHERAL LIGANDS

Many Dy triangular-based motifs have been reported in the literature, and in general, the majority of them have either one or two μ_3-hydroxide or μ_3-oxide as bridging ligands, with a notable structural difference being the peripheral ligands. A quick Cambridge Structural Database (CSD) reveal more than 250 $\{Dy_3\}$ structures reported in the literature, but only a handful of these structures exhibit toroidal moments. As the peripheral ligands are the major difference among the structures reported, the nature and position of donor atoms at the peripheral ligand play a critical role in determining the presence/absence of toroidal moments in the $\{Dy_3\}$ motif. These peripheral ligands connect two Dy centers in each molecule peripherally through their two or three coordination sites. The first Dy_3 toroidal example has been reported by Powell and co-workers that have the *ortho*-vanillin as a peripheral ligand.[1] This complex has the noncollinear alignment of the local anisotropy axes on the three Dy(III) sites and a nonmagnetic ground state that helped them to achieve the SMT behavior predicted by theory and verified by experiments.[2,5] The thorough investigation of the toroidal magnetic moment in the ground state for this parent Dy_3 triangle by experimental and theoretical studies offered an interesting archetype system to explore further and discover other new SMTs and opened up new frontiers in the broader area of SMMs.

Using the *o*-vanillin ligand, Powell and co-workers have synthesized the parent triangular Dy_3 SMT having the formula of $[Dy_3L_3(\mu_3\text{-}OH)_2Cl(H_2O)_5]Cl$ (see Table 1, **1-Dy$_3$**, HL = *o*-vanillin, Figure 2, left).[1] The three Dy(III) centers are connected by two μ_3-OH groups. Furthermore, two Dy(III) ions are bridged by three μ_2-phenoxo groups of *o*-vanillin ligands along each side of the triangle. Likewise, two Cl− ions and two H_2O molecules coordinate to three Dy^{III} ions above and below the triangle plane. Notably, the vanishing susceptibility at low temperature and an S-shaped curve in the *M* vs *H* plot at a lower field at 1.8 K (Figure 2, right) hint at the possibility of a triangular arrangement of the magnetic anisotropy (g_{zz}) axes of each Dy(III) ion. The presence of an S-shaped curve at the magnetization isotherm plot and opening up the hysteresis at low temperature despite having a diamagnetic ground state were puzzling, and the presence of excited states and their associated slow relaxation was suggested as the reason for the puzzling observations.

Chibotaru et al. performed the complete active space self-consistent-field (CASSCF) *ab initio* calculations on the parent Dy_3 triangle molecule to interpret the nature of the nonmagnetic ground state.[2,5] They found that the magnetic anisotropy axes are nearly tangential to the vertices of the triangle (the ϕ angles with the tangential direction are 8.72−9.49°, Figure 2, right, inset) and a small-angle deviation ($\theta = -4.3°$, 8.8°, and −2.4° for Dy1−Dy3, respectively) with the Dy_3 plane. Moreover, the magnetic axes in each Dy site make angles of ca. 120° with each other, and the lowest excited states are illustrated by a large magnetic moment of ca. 20 μ_B. The presence of the $\sim D_{2d}$ symmetry in each Dy(III) site causes the main magnetic anisotropy axes to point outward the Dy_3 triangle. Moreover, the two oxygen atoms lying adjacent to the tangential axis (the OH oxygens of the *o*-vanillin ligands) have a higher negative charge and thus break the D_{2d} symmetry. These results suggested that the deviation of magnetization vectors was primarily influenced by the *o*-vanillin ligand in **1-Dy$_3$** that causes the nonmagnetic ground state and the toroidal arrangement of magnetic moments in each Dy center. The magnetic interaction (exchange and dipolar) between Dy sites supports the noncollinear Ising type that actually preserves the states of maximal magnetizations.

Furthermore, Sessoli et al. performed the single-crystal magnetic measurements combined with theoretical studies to confirm further the magnetic ground state of the **1-Dy$_3$**.[4] Using an ideal model of trigonal symmetry the single-crystal magnetic data were fitted by considering magnetic moments on Dy sites lying in the plane of the molecule. The directions of the magnetic moments on Dy sites have been extracted with the angles $\phi = \pm 17° + n60°$ (n = 0, 1, 2, etc.) with respect to the tangential directions at each Dy center, and the best simulation was achieved corresponding to n = 1. The intramolecular dipolar interaction of magnetic exchange was evaluated as a function of ϕ, and 50% of the contribution was found to come from the most favorable configuration (ϕ = 90°). These results are, in general, in agreement with the results reported by Chibotaru and co-workers.

In 2012, Cheng and co-workers synthesized another triangular Dy_3 SMT different from **1-Dy$_3$** with the formula $[Dy_3(H_2L)(HL)(NO_3)_4]$ (**2-Dy$_3$**, H_4L = *N*,*N*,*N*′,*N*′-tetrakis(2-hydroxyethyl)-ethylene-diamine) using an amino-polyalcohol ligand (H_4L) with four −OH arms.[9] Excluding Dy1···Dy3, sets of Dy(III) ions are singly bridged by a μ_2-O from the H_4L ligand; furthermore, three Dy(III) ions are doubly bridged by two μ_3-O from ligands forming a pseudoisosceles triangle rather than the equilateral triangle, and overall two H_4L ligands and four NO_3^- form this triangle. The transformation of triangular shape owing to the amino-polyalcohol ligand as a peripheral ligand also causes the different magnetic moments and anisotropy axes. Both low-temperature susceptibility and low-field magnetization (Figure 3, right) show non-negligible positive slopes that suggest a nonvanishing magnetic moment in the KD of **2-Dy$_3$** (see Table 1). This condition varies from the parent **1-Dy$_3$** triangle, where the ground state was found to be nonmagnetic;[1] however, this is not the reason for the observation of toroidicity in **2-Dy$_3$**. The orientations of the main magnetic anisotropy axes lie almost in the plane of the Dy_3 triangles where the ϕ angles with the tangential direction are 0.57−10.40°, while these ϕ angles are

https://doi.org/10.1021/acsomega.1c05310
ACS Omega 2021, 6, 32349−32364

Table 1. Summary of All Triangular Shaped SMTs Discussed in This Mini-Review

molecular formula (complex no.)	peripheral ligands[a]	ϕ (deg)[b]	θ (deg)[c]	SMT type	M/μ_B	ref
$[Dy_3L_3(\mu_3\text{-}OH)_2Cl(H_2O)_5]Cl$ (**1-Dy$_3$**)	*o*-vanillin	8.72−9.49	2.4−8.8	mixed moment	0.56	1, 2, 5
$[Dy_3(H_2L)(HL)(NO_3)_4]$ (**2-Dy$_3$**)	*N*,*N*,*N*′,*N*′-tetrakis(2-hydroxyethyl)-ethylene-diamine	0.57−10.4		mixed moment	11.5	9
$[Dy_3(Hpovh)_3(\mu_3\text{-}OH)_2(NO_3)_3(CH_3OH)_2H_2O]\cdot NO_3\cdot 3CH_3OH\cdot 2H_2O$ (**3-Dy$_3$**)	*N*-(pyridyl-methylene)-*o*-vanilloyl-hydrazone (H_2povh)					27
$[Dy_3(H_2vovh)_3(\mu_3\text{-}OH)_2Cl_2(CH_3OH)(H_2O)_3][Dy_3(H_2vovh)_3(\mu_3\text{-}OH)_2Cl_2(H_2O)_4]\cdot Cl_4\cdot 2CH_3OH\cdot 2CH_3CN\cdot 7H_2O$ (**4-Dy$_3$**)	*N*-vanillidene-*o*-vanilloylhydrazone (H_3vovh)					27
$[Dy^{III}_3(teaH_2)_3(OH)(paa)_3]Cl_2$ (**5-Dy$_3$**)	triethanolamine (teaH$_3$) and *N*-(2-pyridyl)-acetoacetamide (paaH)		13	mixed moment	6.4	20
$[Dy_3(o\text{-}dppd)_3(OH)_2Cl_2(H_2O)_4]Cl_2\cdot 7H_2O$ (**6-Dy$_3$**)	1,3-bis(pyridin-2-yl)propane-1,3-dione (*o*-dppdH)		2.8−5.7	mixed moment		28
$[Cr^{III}Dy^{III}_6(o\text{-}tol)_{12}(OH)_8(NO_3)(MeOH)_5]\cdot 3MeOH$ (**7-Cr{Dy$_3$}$_2$**)	*ortho*-toluate	1.1−7.9	0.3−4.7	enhanced FT	9.75	25
$[Dy^{III}_6Mn^{III}(OH)_8(o\text{-}tol)_{12}(MeOH)_5(NO_3)]\cdot 4MeOH$ (**8-Mn{Dy$_3$}$_2$**)	*ortho*-toluate	−2.23		enhanced FT		29
$[Dy^{III}_6Fe^{III}(OH)_8(o\text{-}tol)_{12}(MeOH)_5(NO_3)]\cdot 4MeOH$ (**9-Fe{Dy$_3$}$_2$**)	*ortho*-toluate	−3.82		enhanced AFT	4.4	29
$[Dy^{III}_6Co^{III}(OH)_8(o\text{-}tol)_{12}(MeOH)_5(NO_3)]\cdot 4MeOH$ (**10-Co{Dy$_3$}$_2$**)	*ortho*-toluate	−3.63		enhanced FT	0.01	29
$[Dy^{III}_6Al^{III}(OH)_8(o\text{-}tol)_{12}(MeOH)_5(NO_3)]\cdot 4MeOH$ (**11-Al{Dy$_3$}$_2$**)	*ortho*-toluate	4.58		enhanced FT		29
$[Dy^{III}_6Cr^{III}(OH)_8(o\text{-}tol)_{12}(MeOH)_6]Cl\cdot 6MeOH$ (**7′-Cr{Dy$_3$}$_2$**)	*ortho*-toluate	0.22		enhanced FT		29
$[Dy^{III}_6Mn^{III}(OH)_8(o\text{-}tol)_{12}(MeOH)_6]Cl\cdot 6MeOH$ (**8′-Mn{Dy$_3$}$_2$**)	*ortho*-toluate	−3.66		enhanced AFT		29
$[Dy^{III}_6Fe^{III}(OH)_8(o\text{-}tol)_{12}(MeOH)_6]Cl\cdot 6MeOH$ (**9′-Fe{Dy$_3$}$_2$**)	*ortho*-toluate	1.17		enhanced FT	0.01	29
$[Dy^{III}_6Co^{III}(OH)_8(o\text{-}tol)_{12}(MeOH)_6]Cl\cdot 6MeOH$ (**10′-Co{Dy$_3$}$_2$**)	*ortho*-toluate	−1.68		enhanced FT		29
$[Dy^{III}_6Al^{III}(OH)_8(o\text{-}tol)_{12}(MeOH)_6]Cl\cdot 6MeOH$ (**11′-Al{Dy$_3$}$_2$**)	*ortho*-toluate	−6.40		enhanced FT		29
$\{[Cu(Val)_2CH_3OH][Dy_3L_3(\mu_3\text{-}OH)_2(NO_3)_4]\}_n$ (**12-Cu$_n${Dy$_3$}$_n$**)	enantiopure valine (L- or D-Val), *o*-vanillin	10.3−15.61	0.1−10.2	zero toroidal moment	0.8	8
$[Fe_{18}Dy_6(ampd)_{12}(Hampd)_{12}(\mu\text{-}OH)_6(PhCO_2)_{24}](NO_3)_6\cdot 38MeCN$ (**13-{Fe$_{18}$}{Dy$_3$}$_2$**)	2-amino-2-methyl-1,3-propanediol (H_2ampd)			enhanced FT		26
$[Dy_6L_4L'_2(\mu_3\text{-}OH)_4(H_2O)_9Cl]Cl_5\cdot 15H_2O$ (**14-{Dy$_3$}$_2$**)	*o*-vanillin, 2-hydroxymethyl-6-methoxyphenol	82.1−82.5	<3 and 10	mixed moment		6
$[Dy_6(\mu_4\text{-}O)L_4(NO_3)_4(CH_3OH)]\cdot CH_3OH$ (**15-{Dy$_3$}$_2$**)	2,6-bis((2-hydroxyethylimino)methyl)-4-methylphenol		5.6−9.8	enhanced FT		7
$[Dy_6L_2(\mu_3\text{-}OH)_4(\mu_2\text{-}OH)_2(H_2O)_{12}]\cdot 8Br\cdot 2CH_3CN\cdot 6CH_3OH$ (**16-{Dy$_3$}$_2$**)	4,6-dihydrazinopyrimidine, *o*-vanillin,	2.9−6.9	3.2−7.0	mixed moment		22
$[Dy_6L'_4(\mu_4\text{-}O)(NO_3)_4]\cdot 4CH_3OH$ (**17-{Dy$_3$}$_2$**	2,6-bis((2-hydroxypropyl-imino)methyl)-4-methylphenol					23
$[Cr^{III}Tb^{III}_6(OH)_8(o\text{-}tol)_{12}(NO_3)(MeOH)_5]\cdot 2MeOH$ (**7-Cr{Tb$_3$}$_2$**)	*ortho*-toluate		5.3−13.9	enhanced FT		24
$[Cr^{III}Ho^{III}_6(OH)_8(o\text{-}tol)_{12}(NO_3)(MeOH)_5]\cdot 2MeOH$ (**7-Cr{Ho$_3$}$_2$**)	*ortho*-toluate		5.9−32.4	enhanced FT		24
$[Tb^{III}_3(teaH_2)_3(OH)(paa)_3]Cl_2$ (**5-Tb$_3$**)	triethanolamine (teaH$_3$) and *N*-(2-pyridyl)-acetoacetamide (paaH)		≈2	mixed moment	0.9	20
$[Ho^{III}_3(teaH_2)_3(OH)(paa)_3]Cl_2$ (**5-Ho$_3$**)	triethanolamine (teaH$_3$) and *N*-(2-pyridyl)-acetoacetamide (paaH)		17.7−19.7	mixed moment	6.0	20
$[Tb_3(o\text{-}dppd)_3(CH_3CH_2OH)_3(\mu_3\text{-}OH)_2Cl_3][Tb_3(\mu_3\text{-}OH)_2(o\text{-}dppd)_3(H_2O)(CH_3CH_2OH)_2Cl_3]Cl_2\cdot H_2O$ (**6-Tb$_3$**)	1,3-bis(pyridin-2-yl)propane-1,3-dione (*o*-dppdH)		3.5−35.4	mixed moment		28
$[Ho_3(OH)_2(o\text{-}dppd)_3Cl(H_2O)_5]Cl_3\cdot 3H_2O$ (**6-Ho$_3$**)	1,3-bis(pyridin-2-yl)propane-1,3-dione (*o*-dppdH)		1.9−3.9	mixed moment		28
$[Zn_3Dy_3(\mu_6\text{-}CO_3)(\mu_3\text{-}OH)_3(L)_3(H_2O)_3]\cdot 3(ClO_4)\cdot NO_3$ (**18-Zn$_3$Dy$_3$**)	6,6′-{[2-(dimethylamino) ethylazanediyl]bis(methylene)}bis(2-methoxy-4-methylphenol)	8.9	2.6	net toroidal moment	3.62	30
$[Zn_3Tb_3(\mu_6\text{-}CO_3)(\mu_3\text{-}OH)_3(L)_3(H_2O)_3]\cdot 3(ClO_4)\cdot NO_3$ (**18-Zn$_3$Tb$_3$**)	6,6′-{[2-(dimethylamino) ethylazanediyl]bis(methylene)}bis(2-methoxy-4-methylphenol)	2.4−7.6	4.4−11.2			30

[a]Structure of pheripheral ligands presented in each triangle is shown in their respective figures. [b]ϕ is the angles of magnetic anisotropy axes with tangential direction of the Ln$_3$ triangle. See Figure 2, right, inset. [c]θ is the angle of magnetic anisotropy axes that deviate from the Ln$_3$ triangle.

https://doi.org/10.1021/acsomega.1c05310
ACS Omega 2021, 6, 32349−32364

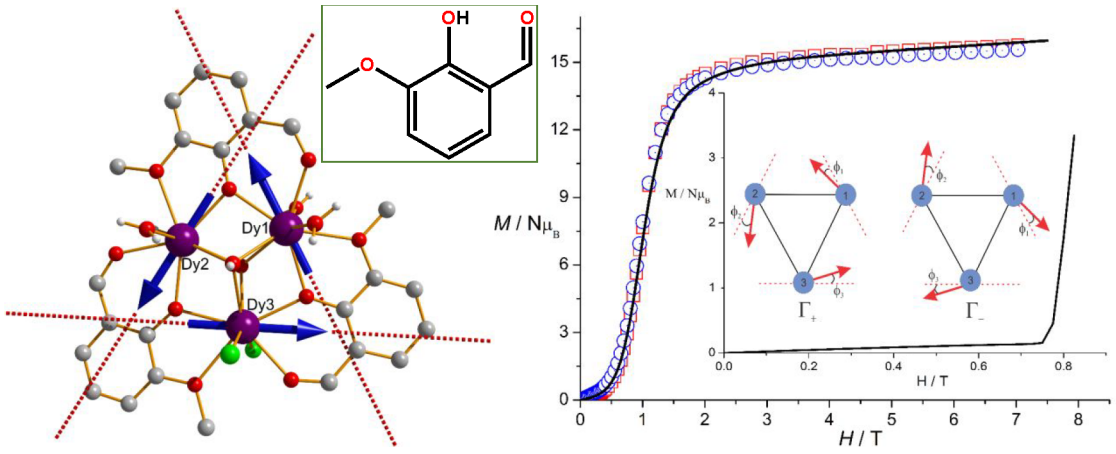

Figure 2. (Left) Structure of the triangular unit in **1-Dy$_3$** with the calculated anisotropy axes (dashed lines) on the Dy sites and the local magnetization (blue arrows) in the ground state. (Right) M vs H calculated and the experimental powder magnetization at T = 1.8 K for **1-Dy$_3$**. Inset: the same simulations for T = 0.1 K and scheme of the two components of the ground Kramers doublet (KD). The arrows show the direction of magnetization on Dy(III) sites. The angles ϕ_I represent the deviation of the resultant anisotropy g_{zz} axis from the tangential direction. Reprinted with permission from ref 5. Copyright 2009, The Royal Society of Chemistry.

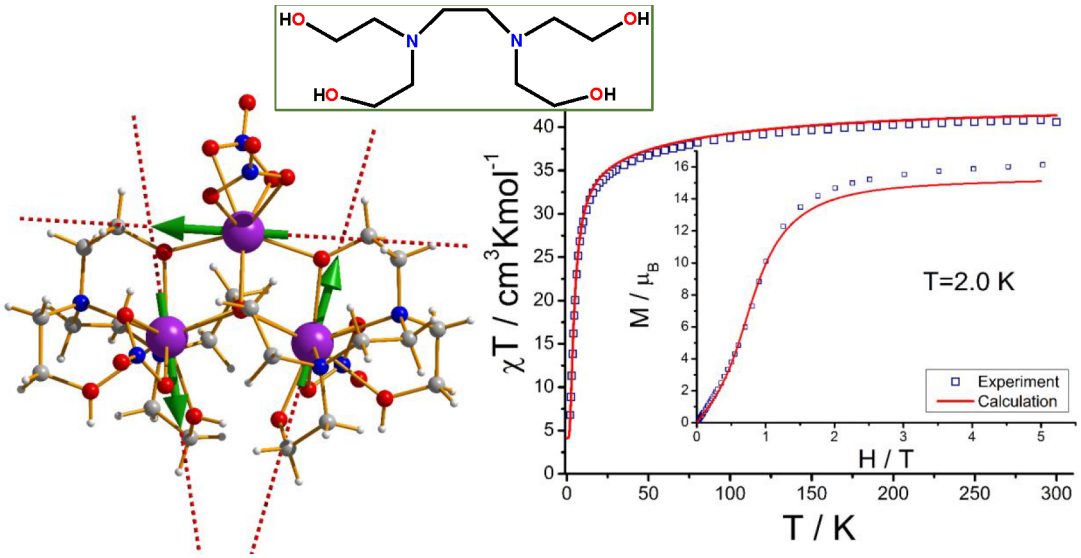

Figure 3. (Left) Molecular structure of **2-Dy$_3$** with g_{zz} axes (dashed lines) and local magnetizations (arrows) in the ground state. (Right) Temperature dependence of the χT. The red line is the *ab initio* calculated curve. Inset: molar magnetization at 2 K for **2-Dy$_3$**. Reprinted with permission from ref 9. Copyright 2012, The Royal Society of Chemistry.

found to be smaller (~9°) in **1-Dy$_3$**. The angles between the main anisotropy in Dy centers are found to be in the range of 25.10−77.97°, whereas this was found to be 120° in **1-Dy$_3$**. As a result, the local magnetic moments in the ground KD do not compensate each other (ca. 11.5 μ_B); thus, the **2-Dy$_3$** remains magnetic until very low temperatures. Overall, the amino-polyalcohol ligand might not be helpful for the nonmagnetic ground state; however, the presence of toroidal magnetic moments was attained. Moreover, *ab initio* calculations suggested that the dipolar interaction alone helps the toroidal alignment of the local magnetic moments. As the dipolar interactions are strongly correlated to the Dy···Dy distance, we envisage that the difference in dipolar interaction and hence the observed toroidicity is likely to be correlated to the presence of an amino-polyalcohol ligand in **2-Dy$_3$**. A similar sign of exchange interactions further stabilizes the circular pattern of local magnetic moments in **2-Dy$_3$**.

In 2012, Tang and co-workers synthesized two more Dy_3 SMTs using the derivatives of the *o*-vanillin ligand.[27] These compounds have been assembled by attaching bulky hydrazine onto the vanillin group, maintaining the vortex-spin structure (Figure 4a and 4b). The two compounds, viz., $[Dy_3(Hpovh)_3(\mu_3\text{-}OH)_2(NO_3)_3(CH_3OH)_2H_2O]\cdot NO_3\cdot 3CH_3OH\cdot 2H_2O$ (**3-Dy$_3$**, H_2povh = *N*-(pyridylmethylene)-*o*-vanilloylhydrazone) and $[Dy_3(H_2vovh)_3(\mu_3\text{-}OH)_2Cl_2(CH_3OH)(H_2O)_3][Dy_3(H_2vovh)_3(\mu_3\text{-}OH)_2Cl_2(H_2O)_4]\cdot Cl_4\cdot 2CH_3OH\cdot 2CH_3CN\cdot 7H_2O$ (**4-Dy$_3$**, H_3vovh = *N*-vanillidene-*o*-vanilloylhydrazone), have a similar two μ_3-OH bridged triangular archetype as observed in **1-Dy$_3$**. The observed structural differences between these two structures and the parent **1-Dy$_3$** structure resulted in different dynamic magnetic behavior revealed by their AC susceptibility. Even though the theoretical calculations are not performed on these complexes, both the vanishing susceptibility at low temperature and the noticeable S-shaped curve at the lower

https://doi.org/10.1021/acsomega.1c05310
ACS Omega 2021, 6, 32349−32364

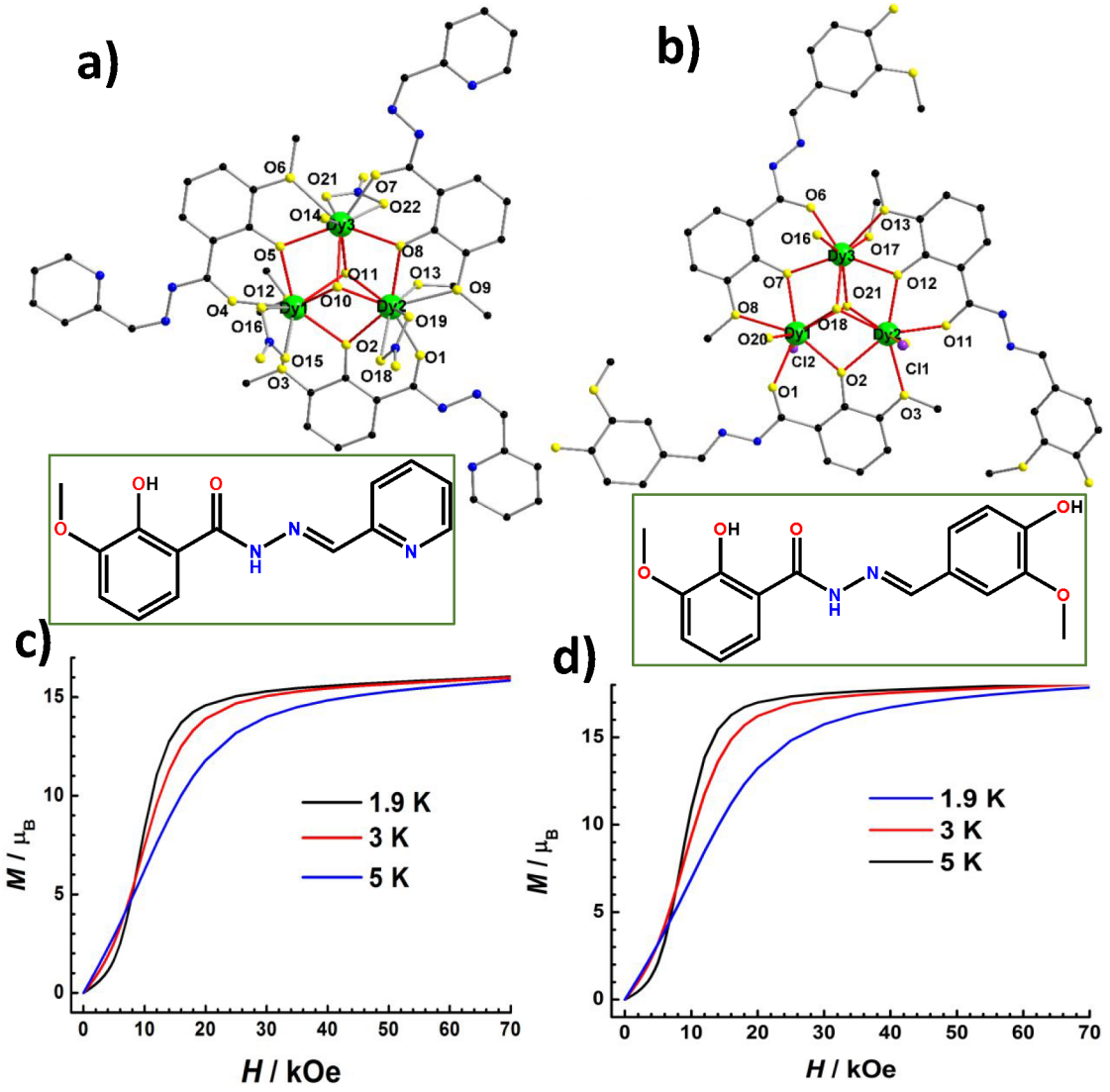

Figure 4. Molecular structure of (a) **3-Dy$_3$** and (b) **4-Dy$_3$**. Field dependences of magnetization for (c) **3-Dy$_3$** and (d) **4-Dy$_3$**. Reprinted with permission from ref 27. Copyright 2012, Americal Chemical Society.

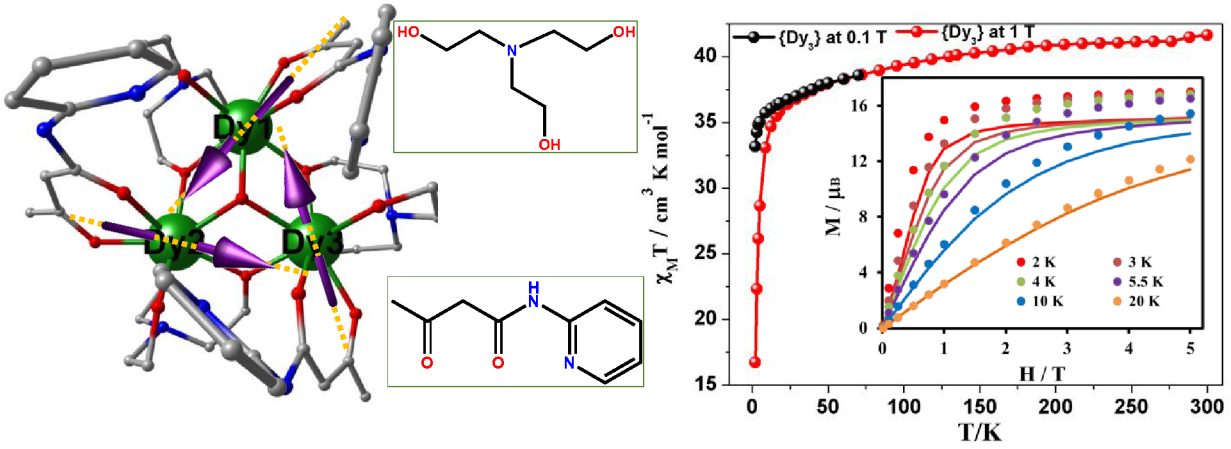

Figure 5. (Left) Molecular structure and the orientations of the magnetic anisotropy axes in the ground doublets on the Dy^{III} sites in **5-Dy$_3$**. (Right) χT vs T plots for **5-Dy$_3$** in an applied dc field of 0.1 and 1 T. (Inset) The molar magnetization data for **5-Dy$_3$**. The solid lines are calculated data. Reprinted with permission from ref 20. Copyright 2019, The Royal Society of Chemistry.

field in M vs H plots suggest a nonmagnetic ground state (Figure 4c and 4d). This might suggest that these two complexes possess a toroidal magnetic moment. Since these two complexes possess the derivative of the *o*-vanillin ligand, we envisage that they could

https://doi.org/10.1021/acsomega.1c05310
ACS Omega 2021, 6, 32349−32364

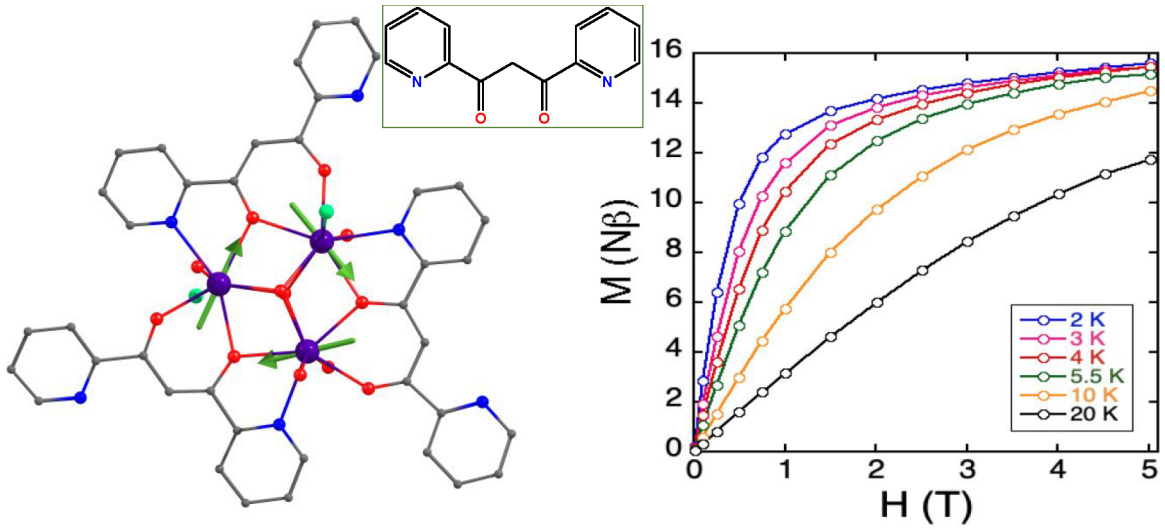

Figure 6. (Left) Molecular structure and arrangement of the anisotropic axis (green and black arrows) for the ground-state KDs in **6-Dy$_3$**. Violet = Dy, Red = O, Gray = C, Blue = N, Green = Cl. (Right) Magnetization isotherms (2−20 K) in applied fields 0−5 T for **6-Dy$_3$**. Reprinted with permission from ref 28. Copyright 2020, The Royal Society of Chemistry.

also show similar kinds of magnetic anisotropy axes tangential to the vertices of the Dy_3 triangle and a small-angle deviation to the Dy_3 plane; however, this can not be confirmed as *ab initio* calculations or experimental verifications are lacking.

In 2019, Langley et al. reported the magnetic and theoretical characteristics of a triangular Dy complex (Figure 5a), $[Dy^{III}_3(teaH_2)_3(OH)(paa)_3]Cl_2$ (**5-Dy$_3$**; $teaH_3$ = triethanolamine and paaH = *N*-(2-pyridyl)-acetoacetamide], along with their Tb and Ho analogues.[20] The three Dy ions are bridged by a μ_3-OH ligand, and the three triethanolamine ligands connecting Dy ions via one O-atom of the singly deprotonated −OH arm and two protonated −OH arms and the N-atom chelate. Each paa^- ligand chelates to one Dy^{III} ion through the β-diketonate functionality. An essential structural alteration between the parent **1-Dy$_3$** and **5-Dy$_3$** is the presence of two μ_3-OH bridging ligands in **1-Dy$_3$**, whereas this complex has just one central μ_3-OH bridge. An S-shaped curve was not observed for **5-Dy$_3$** in the *M* vs *H* plots in low fields (Figure 5, right, inset); however, *ab initio* CASSCF calculations predict that this **5-Dy$_3$** molecule exhibits SMT behavior. The magnetic anisotropy axes are found to lie closer to the Dy_3 plane, with a deviation angle (θ) of 13° observed, and the same is found to be in the range of 2.4−8.8° for **1-Dy$_3$**.[1] These axes are almost tangential to the vertices of the Dy_3 triangle, similar to **1-Dy$_3$**, which affirms the presence of a toroidal magnetic moment. As a consequence, noncollinear arrangement between localized magnetic moments owing to the presence of dipolar interactions does not compensate each other, resulting in a small magnetic moment (ca. 6.4 μ_B), which is three times smaller compared to the value calculated for the **1-Dy$_3$** (~20 μ_B). This result agrees well with the observation of nonvanishing susceptibility at low temperature (Figure 5, right) as observed in **2-Dy$_3$**.[9] In this example as well, the toroidal magnetic moments are found to be favored by both dipolar and exchange interactions, both of which are controlled by the peripheral triethanolamine ligand. As triethanolamine is also an amino-polyalcoholic ligand, it appears that such ligands favor mixed magnetic moments of the toroidal ground state, as observed in **2-Dy$_3$** having a similar ligand framework.[9,10]

In 2020, Caporale et al. have reported a different Dy_3 SMT and characterized their toroidal behavior using magnetic instruments and *ab initio* calculations.[28] This complex having the formula of $[Dy_3(o\text{-dppd})_3(OH)_2Cl_2(H_2O)_4]Cl_2{\cdot}7H_2O$ (**6-Dy$_3$**, Figure 6, left) has been synthesized using a pyridyl-containing β-diketonate, 1,3-bis(pyridin-2-yl)propane-1,3-dione (*o*-dppdH). Each β-diketonate ligand chelates two Dy^{III} centers where one O-atom is shared (μ_2-O) between the two Dy^{III} centers, and the other O-atom binds solely to one Dy^{III} atom. Likewise, a pyridyl nitrogen atom coordinates to each Dy^{III} center; however, the other pyridyl nitrogen atom is left unbound. Importantly, all three Dy^{III} centers are bridged by two central μ_3-OH ligands that lie above and below the Dy_3 plane. Like *o*-vanillin Dy_3 systems (**1-Dy$_3$**), this complex also possesses a triangular dodecahedron geometry with D_{2d} symmetry. The S-shaped curve in the *M* vs *H* plot at low fields is not observed. However, *ab initio* calculations predict that orientations of the magnetic anisotropy axes in each Dy center in the ground state form a circular pattern, suggesting SMT behavior for **6-Dy$_3$**. The localized molecular polarizability charge is higher at the bridging O of the diketo group and less for μ_3-O, which makes the g_z axis lie in the direction of the bridging keto oxo group and helps to form the circular pattern of the anisotropy axis in **6-Dy$_3$**. Moreover, with the small energy gap at the first excited state, the **6-Dy$_3$** loses its toroidal arrangement due to the alteration of direction of the anisotropy axis in one of the Dy centers, which could be the reason for not observing the S-shaped curve in the *M* vs *H* plot. The ground-state magnetization vectors are found to lie nearly in the Dy_3 plane with a small angle of deviation (θ = 2.8°, 3.0°, and 5.7° for **Dy$_1$−Dy$_3$**, respectively), and these are similar to the values obtained for the *o*-vanillin Dy_3 systems (**1-Dy$_3$**).[1] The presence of the D_{2d} symmetry at each Dy(III) site and a huge negative charge on the O atom of the diketo group enforce the anisotropic g_z axis to lie along with this bond which is tangential to the vertices of the Dy_3 triangle. This observation is very similar to the one found for **6-Dy$_3$**.

DOUBLE {DY$_3$} TRIANGLES CONNECTING VIA 3D IONS

It is reported that two Dy_3 triangles displaying toroidal states are connected via a 3d ion or by peripheral ligands. In that case, the two toroidal moments can lead to enhanced toroidal moments,

https://doi.org/10.1021/acsomega.1c05310
ACS Omega 2021, 6, 32349−32364

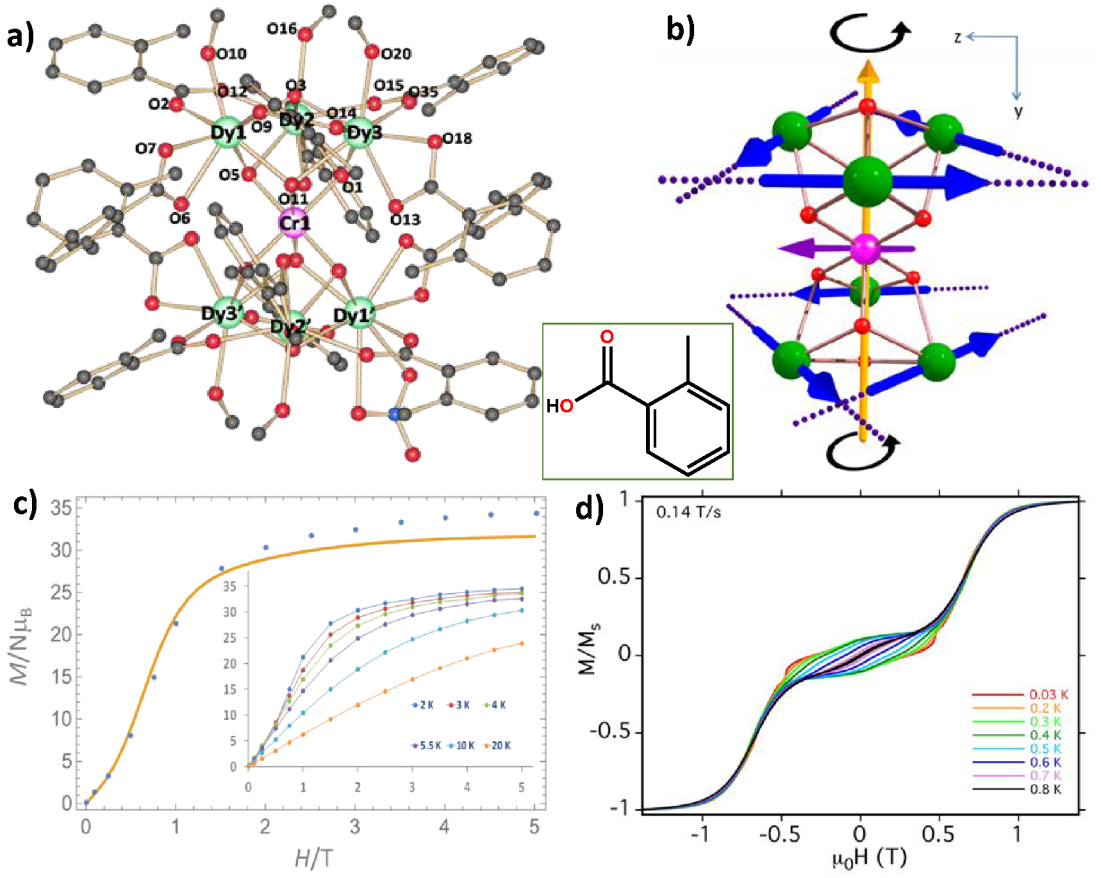

Figure 7. (a) Molecular structure of 7-**Cr{Dy$_3$}$_2$**. (b) The orientations of the g_{zz} axes in the ground KD on each Dy site (dotted lines) in 7-**Cr{Dy$_3$}$_2$**. Blue arrows are the local magnetic moment in the ground KD. The con-rotation of the toroidal magnetic moment is shown by black arrows, and the yellow arrow is the S_6 symmetry axis. (c) The measured (blue circles) and simulated (orange solid line) plot of an M vs H isotherm at 2 K for 7-**Cr{Dy$_3$}$_2$**. (Inset) M vs H isotherms for 7-**Cr{Dy$_3$}$_2$** at 2, 3, 4, 5.5, 10, and 20 K. (d) MicroSQUID magnetization (M) vs applied field plot for 7-**Cr{Dy$_3$}$_2$** at a 0.03−0.8 K with the scan rate of 0.14 T s^{-1}. Reprinted with permission from ref 25. Copyright 2017, Nature Publishing Group.

an essential criterion for realizing potential applications proposed for molecular ferrotoroidicity and the development of molecule-based multiferroics.[7,8,10,15,25] There are a few examples where two Dy_3 triangles connected by the peripheral ligands have been reported.[6,7,22,23] In order to isolate a complex with a ferrotoroidal ground state, we have focused our attention on {3d−4f} coordination complexes containing anisotropic Dy ions and transition metal ions such as Cr(III).[25]

{Dy$_3$}−Cr−{Dy$_3$} Motif to Achieve Ferrotoroidicity. We have synthesized and theoretically studied a heptanuclear {$CrDy_6$} complex, viz., $[Cr^{III}Dy^{III}_6(o\text{-tol})_{12}(OH)_8(NO_3)(MeOH)_5]\cdot 3MeOH$ (7-**Cr{Dy$_3$}$_2$**, *o*-tol = *ortho*-toluate).[25] It has been found that the metallic core is two triangular Dy^{III} motifs that lie above and below a single central Cr^{III} ion (Figure 7a and 7b), and it is stabilized by 8 μ_3-OH and 12 *o*-tol, MeOH, and $[NO_3]^-$ ligands. Two μ_3-OH ligands bridge the three Dy^{III} ions and form each triangle, whereas the other six μ_3-OH ligands bridge two Dy^{III} ions to the central Cr^{III} ion. The 7-**Cr{Dy$_3$}$_2$** displays an S-shaped curve at 2 and 3 K at low fields in M vs H plots (Figure 7c) and a stepped shape of the magnetization in single-crystal micro-SQUID measurements (Figure 7d), which proposes the presence of a toroidal moment.[10,12] This {$CrDy_6$} complex displays slow magnetic relaxation and SMM behavior at temperatures below 2 K. Theoretical studies predict that the 7-**Cr{Dy$_3$}$_2$** complex shows a very rare ferrotoroidically (FT) coupled ground state determined by dipolar coupling between the two con-rotating toroidal Dy_3 triangles. A pseudo S_6 axis passes via the Cr^{III} ion and the center of both of the {Dy^{III}_3} triangular motifs (Figure 7b). The calculated anisotropy axes are found to lie in the Dy_3 plane with an out-of-plane angle (θ) of 0.3, 4.5, and 4.7° for Dy1, Dy2, and Dy3, respectively. These calculated g_{zz} axes are perfectly aligned with the tangents to an ideal circumference enclosing the triangles (the ϕ angle of the anisotropy axis with these tangential directions is in the range of 1.1−7.9°). These values are almost similar to the values calculated for the parent **1-Dy$_3$**. By comparing the hysteresis profile of 7-**Cr{Dy$_3$}$_2$** with the parent **1-Dy$_3$** toroidal complex,[1] we find that the profile is superior for the former, particularly comparing the coercitivity. This finding suggests that coupling between the two Dy_3 triangles in 7-**Cr{Dy$_3$}$_2$** enhances the toroidal magnetic moment due to the presence of the ferrotoroidically coupled ground state.[25] The dipolar-induced FT/AFT (antiferrotoroidal) splitting is calculated as ∼0.28 cm^{-1}, and the spin of Cr(III) is freely fluctuating.

While ferrotoroidal behavior was achieved in 7-**Cr{Dy$_3$}$_2$**, the next reasonable question was how the connecting 3d ion would affect the ferrotoroidal behavior. Some of us have isolated another {$CrDy_6$} complex with a different counteranion (chloride) and other 3d/p block ions as a central metal that connects two Dy_3 triangles to enhance the ferrotoroidal coupling.[29] The family of complexes may differ in the counteranion and has the general molecular formula of $[Dy^{III}_6M^{III}(OH)_8(o\text{-tol})_{12}(MeOH)_5(NO_3)]\cdot 4MeOH$ (M = Mn (**8-Mn{Dy$_3$}$_2$**), Fe (**9-Fe{Dy$_3$}$_2$**), Co (**10-Co{Dy$_3$}$_2$**),

https://doi.org/10.1021/acsomega.1c05310
ACS Omega 2021, 6, 32349−32364

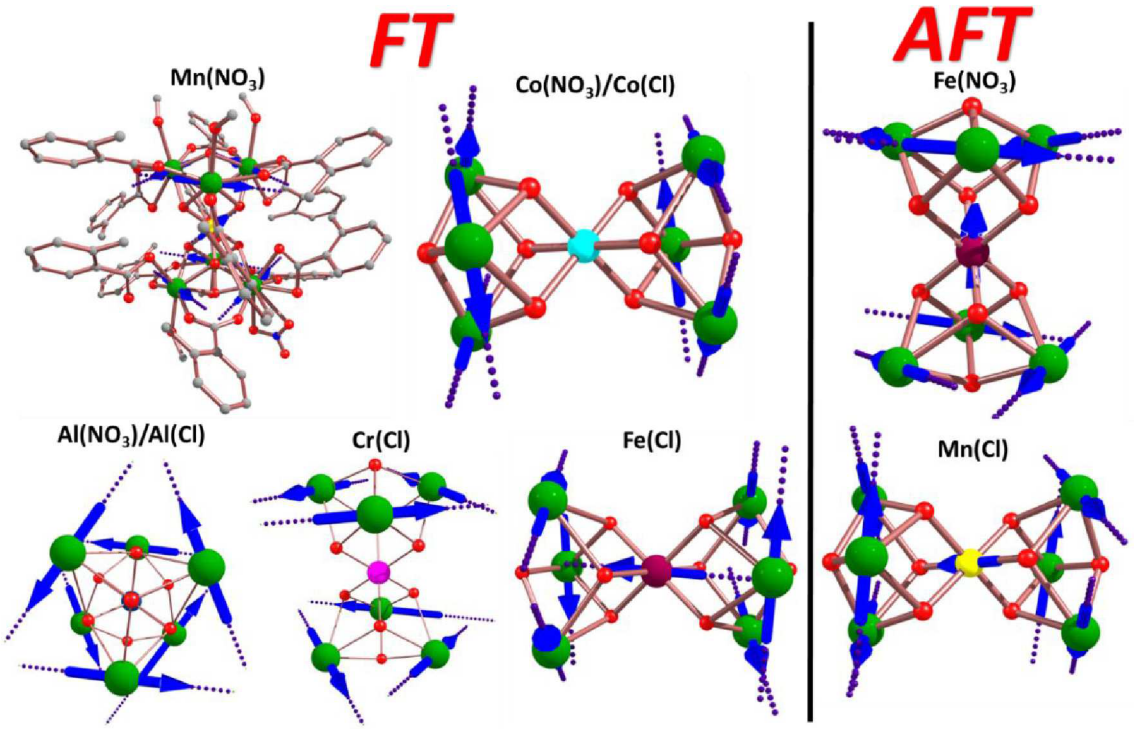

Figure 8. Orientations of magnetic anisotropy axes (dotted lines and blue arrows) in each MDy_6 complex.

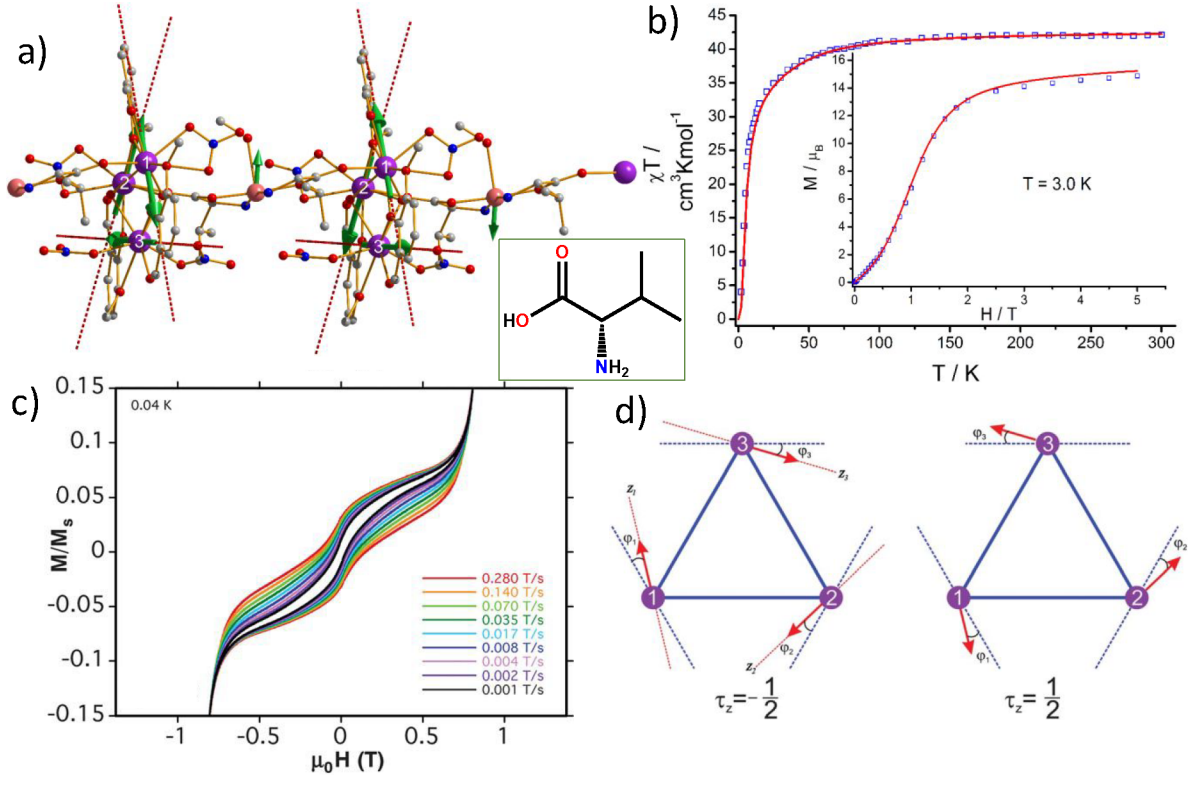

Figure 9. (a) Molecular structure of **12-Cu$_n${Dy$_3$}$_n$** along with the calculated g_{zz} axes for the lowest KDs on Dy ions in the D-chain; (b) measured and calculated magnetic susceptibility data and molar magnetization at 3.0 K for the D-chain; (c) microSQUID magnetization (M) vs applied field plot for the D-chain (bottom) with different field sweep rates at 0.04 K; and (d) two components of the toroidal state $\tau = 1/2$ of the Dy_3 triangles. Blue dashed lines show the tangential directions, and red dashed lines are the anisotropy axes. Reprinted with permission from ref 8. Copyright 2012, The Royal Society of Chemistry.

and Al (**11-Al{Dy$_3$}$_2$**); *o*-tol = *o*-toluate) and $[Dy^{III}_6M^{III}(OH)_8(o\text{-tol})_{12}(MeOH)_6]Cl{\cdot}6MeOH$ (M = Cr (**7′-Cr{Dy$_3$}$_2$**), Mn (**8′-Mn{Dy$_3$}$_2$**), Fe (**9′-Fe{Dy$_3$}$_2$**), Co (**10′-Co{Dy$_3$}$_2$**), and Al (**11′-Al{Dy$_3$}$_2$**), see Table 1). Despite that

https://doi.org/10.1021/acsomega.1c05310
ACS Omega 2021, 6, 32349−32364

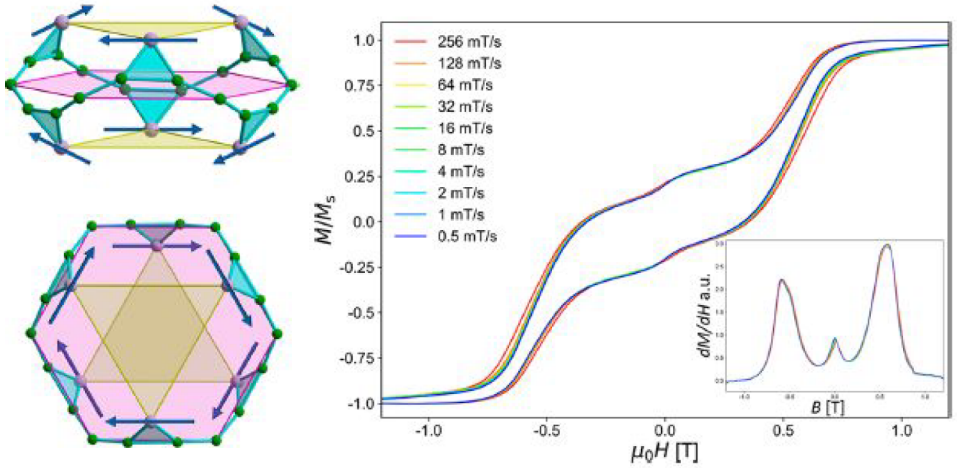

Figure 10. (Left) $Fe_{18}Dy_6$ metallic core with the arrangement of g_{zz} axis (dark blue) within the Dy_3 triangles sandwiching the Fe_{18} ring. (Right) MicroSQUID magnetic hysteresis of **13-{Fe$_{18}$}{Dy$_3$}$_2$** at 30 mK under varying field sweep rates and derivative. (Inset) The loops show a plateau between −0.5 and 0.5 T. Reprinted with permission from ref 26. Copyright 2020 Americal Chemical Society.

the Cr(III) ion is substituted by various metal ions, the core $\{Dy_3O\}$ structure is found to be retained in all geometries, offering a possibility to observe ferro-/antiferrotoroidicity in this class of molecule. Each Dy^{III} ion's magnetic anisotropy axis almost lies in-plane and tangentially to a $\{Dy_3\}$ triangle in all the complexes. The Dy^{III} magnetic axes form circular patterns, suggesting toroidal ground states in both the triangles (Figure 8). Complexes Cr(Cl)/Mn(NO_3)/Fe(Cl)/Co(Cl)/Co(NO_3)/Al(Cl)/Al(NO_3) have their magnetic moments oriented clockwise in both the triangles, leading to the FT ground state, but the complexes Mn(Cl)/Fe(NO_3) have their magnetic moment oriented anticlockwise in one of the Dy_3 triangles leading to an AFT ground state. Importantly, the theoretical calculations confirmed that the ground-state toroidal behavior depends on the nature of the magnetic coupling between the Dy^{III} ions, which is consistent with the experimental observation. Above all, we have revealed that: (i) the ferrotoroidic coupling between Dy_3 motifs can be enhanced by small, diamagnetic M linking ions; (ii) a paramagnetic M ion is able to stabilize the antiferrotoroidic states only if the anisotropy is held up; and (iii) by choosing a better M ion, a complex's hysteresis profile can be fine-tuned to increase the remnant magnetization and/or coercive field. Moreover, a model to simulate microSQUID hysteresis plots was developed for the first time in this work. This tool helps to validate the presence/absence of the ferro/antiferrotoroidal arrangement.[29]

Cu{Dy$_3$}$_n$ Polymer Exhibiting Antiferrotoroidicity. The coupling of two or more triangular Dy_3 rings via a 3d ion, each stabilizing a toroidal moment in their ground state, has been first explored by Powell and co-workers in a chiral heterometallic polymer having the formula of $\{[Cu(Val)_2CH_3OH][Dy_3L_3(\mu_3\text{-}OH)_2(NO_3)_4]\}_n$ (**12-Cu$_n${Dy$_3$}$_n$**, Val = enantiopure valine (L- or D-Val), HL = *o*-vanillin; Figure 9a).[8] They have reported the first Cu^{II}/Dy^{III} 1D polymers built from an alternating trinuclear Dy_3 SMT-building motif and a Cu(II) bisvalinate complex with the chiral spin state propagating along the chain, which exhibits the exchange coupling between the toroidal moments. The **12-Cu$_n${Dy$_3$}$_n$** displays an S-shaped curve in magnetization isotherm plots at low fields and low temperatures (Figure 9b) and a stepped hysteresis of the magnetization (Figure 9c) in single-crystal studies. *Ab initio* calculations predict the antiferromagnetic coupling between Dy ions, thus allowing the local magnetic moments to be arranged in a toroidal fashion (Figure 9a and 9d). The main g_{zz} axes on Dy sites are adjacent to tangential directions with angles (ϕ) of 10.3−15.61° (Figure 9d), and they lie nearly in the Dy_3 plane with a deviation (θ) of 0.1−10.2°. These values are comparable to the values found for the ground state of the parent **1-Dy$_3$** triangle, thus showing well-maintained toroidal moments within the individual $\{Dy_3\}$ motif despite the polymerization of the Dy_3 units, and they have uncompensated moments (0.8 μ_B). They also showed how to induce strong toroidal magnetization by applying a magnetic field at low temperature in single crystals of these compounds. The ground state of such a system is found to be antiferrotoroidic, and it is argued there that the ferrotoroidic first excited state, having a magnetic component, can be stabilized by a magnetic field, so that in an applied magnetic field condition in the appropriate direction the ground state would become ferrotoroidic (but not degenerate).

{Fe$_{18}$}{Dy$_3$}$_2$ Exhibiting Ferrotoroidicity. Recently, Powell and co-workers reported a large $\{Fe_{18}Dy_6\}$ cyclic coordination cluster, viz., $[Fe_{18}Dy_6(ampd)_{12}(Hampd)_{12}(\mu\text{-}OH)_6(PhCO_2)_{24}](NO_3)_6\cdot 38MeCN$ (**13-{Fe$_{18}$}{Dy$_3$}$_2$**, H_2ampd = 2-amino-2-methyl-1,3-propanediol).[26] In this molecule, two giant Dy_3 triangles were sandwiched by a strongly antiferromagnetically coupled Fe_{18} ring, and it shows a ferrotoroidal behavior in the ground state (Figure 10, left). The cluster is possibly fragmented into repeating $\{Fe_2Dy\}$ triangles connected via a benzoate-bridged Fe ion to form a "modified delta-chain". Therefore a $\{Fe_3Dy\}$ moiety is a repeating unit within the chain. Though the dominant interaction in the Fe_{18} ring is antiferromagnetic, the six Dy ions arrange themselves toroidally. No clear evidence for an S-shaped curve in the *M* vs *H* plots was noted; however, the toroidal arrangement was ascertained by microSQUID measurements (Figure 10, right). If we compare the microSQUID data for the ferrotoroidal **7-Cr{Dy$_3$}$_2$** complex[25] and that of the **13-{Fe$_{18}$}{Dy$_3$}$_2$**, very similar features are observed. The microSQUID hysteresis loops display a plateau between −0.5 and 0.5 T, which is representative of a nonmagnetic toroidal ground state. Quantum calculations found that the moments are arranged ferrotoroidally. Moreover, the field needed to break

https://doi.org/10.1021/acsomega.1c05310
ACS Omega 2021, 6, 32349−32364

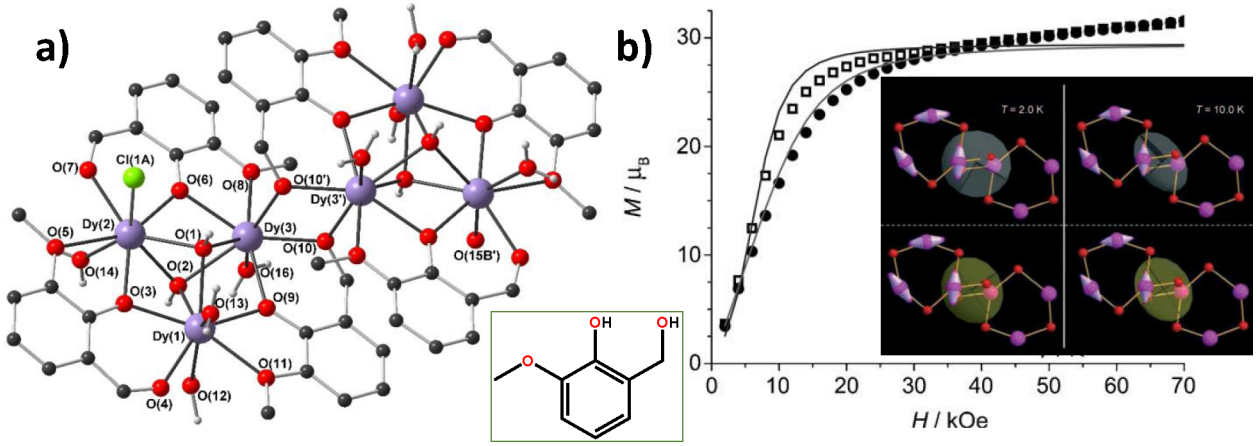

Figure 11. (a) Structure of the $\{Dy_6\}^{5+}$ cation in **14-**$\{\mathbf{Dy_3}\}_2$. (b) Field dependence of the molar magnetization measured of **14-**$\{\mathbf{Dy_3}\}_2$ at T = 1.8 K (□) and T = 4.0 K (●). Inset: Ellipsoidal representation of the experimental (top) and calculated (bottom) susceptibility tensors of Dy_6 at two different temperatures. The tensors are superimposed onto the molecular structure of the magnetic core (Dy violet, O red); the orientation of the Dy easy axes estimated from *ab initio* calculations is also shown. Reprinted with permission from ref 6. Copyright 2010, John Wiley & Sons Ltd.

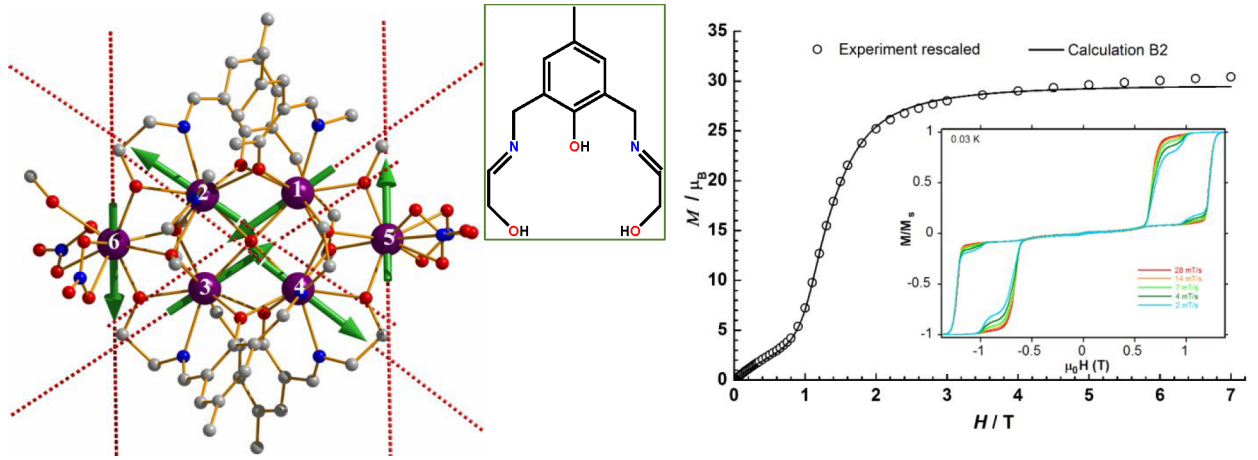

Figure 12. (Left) Molecular structure of **15-**$\{\mathbf{Dy_3}\}_2$ with the main anisotropy axes (dashed lines) on Dy ions and local magnetizations (arrows) in the ground state. (Right) M vs H at 1.9 K. The solid line corresponds to the best fit. Inset: Hysteresis loops for **15-**$\{\mathbf{Dy_3}\}_2$ at different field sweep rates at 0.03 K. Reprinted with permission from ref 7. Copyright 2012, John Wiley & Sons Ltd.

the toroidal arrangement in the **13-**$\{\mathbf{Fe_{18}}\}\{\mathbf{Dy_3}\}_2$ system is nearly as large as that for the **7-Cr**$\{\mathbf{Dy_3}\}_2$ (*vide infra*).

DOUBLE $\{DY_3\}$ TRIANGLES CONNECTED VIA PERIPHERAL LIGANDS

After the remarkable observation of SMT behavior in the parent Dy_3 triangle, in 2010, Powell and co-workers purposely added a 2-hydroxymethyl-6-methoxyphenol ligand and discovered a $\{Dy_6\}$ cluster with two Dy_3 units coupled with each other (Dy_3 + Dy_3 connected by an inversion center in a vertex-to-vertex fashion) having the formula of $[Dy_6L_4L'_2(\mu_3\text{-}OH)_4(H_2O)_9Cl]Cl_5{\cdot}15H_2O$ (**14-**$\{\mathbf{Dy_3}\}_2$, HL = *o*-vanillin, and H_2L' = 2-hydroxymethyl-6-methoxyphenol).[6] This Dy_6 structure results from the formal linkage by the alkoxides of the reduced form of the ligand ($-CH_2OH$ from H_2L') of two Dy_3 triangles in **1-**$\mathbf{Dy_3}$ with the associated formal loss of the two terminal Cl^- ligands (Figure 11a). In the M vs H plots, an S-shaped curve is observed at 1.8 K at 0.5 kOe (Figure 11b), and this behavior is mostly comparable to that of the parent **1-**$\mathbf{Dy_3}$ cluster; however, the antiferromagnetism is less pronounced due to the presence of an even number of interacting Dy centers.

The calculated directions of the anisotropy axes for Dy_1 and Dy_2 centers in **14-**$\{\mathbf{Dy_3}\}_2$ lie almost in the Dy_3 plane (deviation (θ) of <3°) and are tangential to the triangle. These outcomes are consistent with the **1-**$\mathbf{Dy_3}$ when the similar ligand environments of Dy_1 and Dy_2 are found in both the compounds. However, for the central Dy_3 ions, the g_{zz} easy-axis deviates by about 10° from the plane of the triangle, replicating the slightly different coordination surroundings resulting from the alkoxo bridges to the second triangle (Figure 11b, inset). Furthermore, the weak interaction between the two triangles could not stabilize the con-rotating or counter-rotating of the magnetic moments in each triangle. It means that the total toroidal moment of **14-**$\{\mathbf{Dy_3}\}_2$ is not maximized by such coupling, as the antiferromagnetic interwheel interaction is such that it cancels the contribution arising from the Dy magnetic moment of the two coupled vertices to the overall vortex magnetization. In terms of con-rotating and counter-rotating toroidal moments on the two triangular subunits, the FT and/or AFT nature of such states was not explicitly discussed. Given that FT and AFT states are nonmagnetic, they make little contribution to the magnetic response of the system. In this respect, the fact that the Hamiltonian used in this work contains four fitting parameters

https://doi.org/10.1021/acsomega.1c05310
ACS Omega 2021, 6, 32349−32364

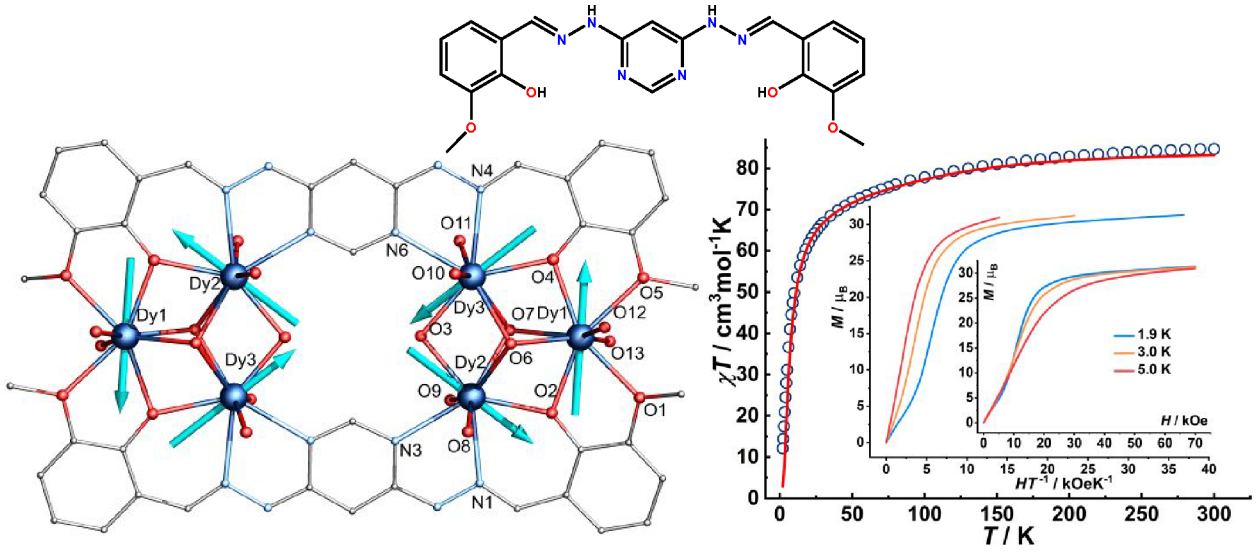

Figure 13. (Left) Structure with main anisotropy axes (dashed lines) and local magnetizations (arrows) in the ground state and (right) magnetic plots of **16**-$\{Dy_3\}_2$. Reprinted with permission from ref 22. Copyright 2016, The Royal Society of Chemistry.

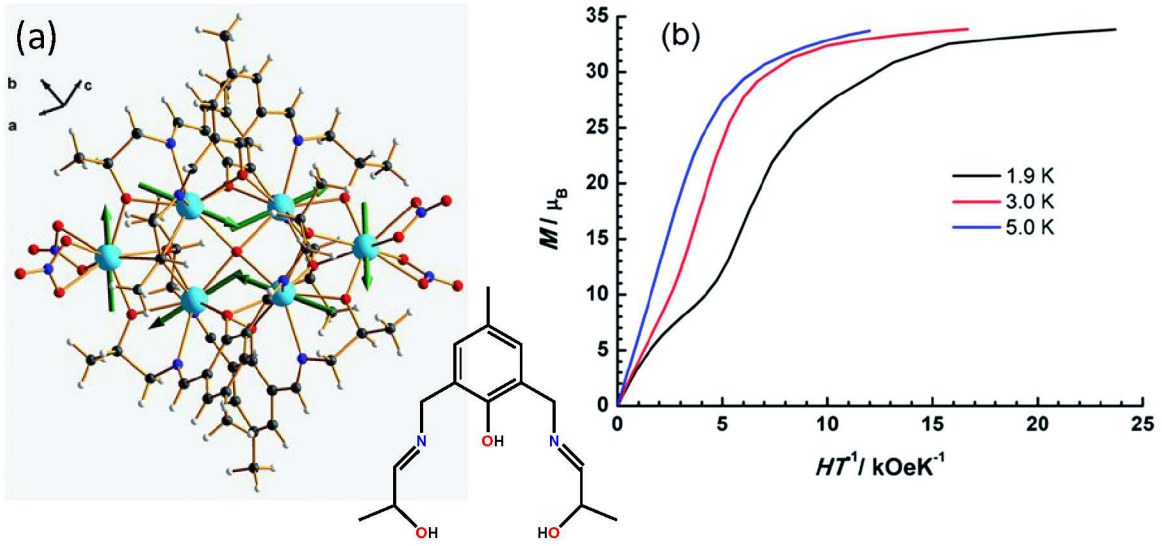

Figure 14. (a) Structure with main anisotropy axes (dashed lines) and local magnetizations (arrows) in the ground state and (b) *M* vs *H* plot of **17**-$\{Dy_3\}_2$. Reprinted with permission from ref 23. Copyright 2017, The Royal Society of Chemistry.

and neglects dipolar coupling suggests that more detailed investigations of **14**-$\{Dy_3\}_2$ are necessary to affirm the presence/absence of the FT ground state.

After succeeding in linking the two Dy_3 units in a vertex-to-vertex fashion in the **14**-$\{Dy_3\}_2$ molecule, in 2012, Powell and co-workers have reported another Dy_6 molecule (Figure 12, left) coupling two Dy_3 units ($[Dy_3(\mu_3\text{-}O)_2(\mu_2\text{-}O)_2]$) but in an edge-to-edge fashion, viz., $[Dy_6(\mu_4\text{-}O)L_4(NO_3)_4(CH_3OH)]\cdot CH_3OH$ (**15**-$\{Dy_3\}_2$, H_3L = 2,6-bis((2-hydroxyethylimino)methyl)-4-methylphenol).[7] The alcohol μ_2-O atoms from the same ligands (H_3L) bridge the edges of the triangles. Notably, the μ_4-O^{2-} ion connects two Dy_3 triangles in the center, and four deprotonated phenol oxygen atoms further merge the Dy_6 molecule in the edge to organize the two Dy_3 triangles in an edge-to-edge arrangement. The measured magnetization with a variable field at 1.9 K shows a pronounced S-shape around 9 kOe, and a stepped shape of the magnetization hysteresis in the micro-SQUID technique indicates the presence of toroidal behavior (Figure 12, right). The reason for the presence of a large magnetic moment is due to the orientations of local anisotropy axes (perfectly arranged in a toroidal fashion in both triangles), which vary much more from an equilateral triangle in this compound than in the parent **1**-Dy_3, and the presence of much lower symmetry for this Dy_6. Thus, this Dy_6 construction enhanced the toroidal magnetic moment of the molecule.

In particular, we note that while antiferromagnetic coupling between Dy^{III} ions belonging to the same triangle is known to stabilize a toroidal moment, given the geometry of **15**-$\{Dy_3\}_2$, antiferromagnetic coupling between nearest-neighbor ions on different triangles will in fact stabilize counter-rotating toroidal states on different triangles, hence an antiferrotoroidic ground state. The lack of low-lying antiferrotoroidic excitations renders this system a somewhat less clear-cut case of a well-defined magnetic coupling between separate toroidal subunits, such as the case presented in **7**-**Cr**$\{Dy_3\}_2$,[25] albeit an exciting example of how to achieve a large toroidal moment in the ground state.

In 2016, Cheng and co-workers also had reported a Dy_6 molecule by linking two Dy_3 triangles, viz., $[Dy_6L_2(\mu_3\text{-}OH)_4(\mu_2\text{-}$

https://doi.org/10.1021/acsomega.1c05310
ACS Omega 2021, 6, 32349−32364

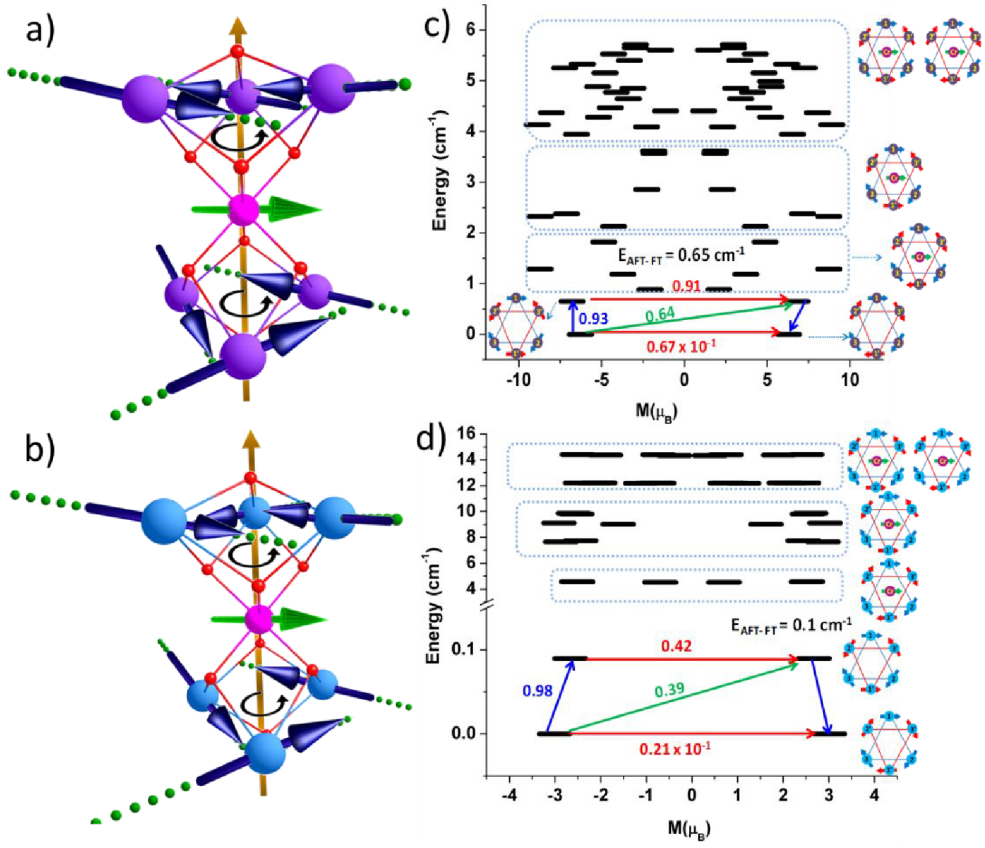

Figure 15. Metallic core with the direction of the local anisotropy axes (green dotted lines) and the local magnetic moment (blue arrows) in the ground Ising doublet on each Tb^{III} and Ho^{III} site in **7-Cr{Tb$_3$}$_2$** (a) and **7-Cr{Ho$_3$}$_2$** (b). The blue arrows show the con-rotation of the toroidal magnetic moment, and and the yellow arrow is the S_6 symmetry axis. Low-lying exchange spectrum for (c) **7-Cr{Tb$_3$}$_2$** and (d) **7-Cr{Ho$_3$}$_2$**. The exchange-coupled states (KDs) are placed on the diagram according to their magnetic moments (bold black lines). For various energy states, a graphical representation of one of the corresponding noncollinear Ising quantum states, where the red/blue thick arrows at the Ln^{III} sites indicate the direction of the magnetic moment in toroidal form. Reprinted with permission from ref 24. Copyright 2018, John Wiley & Sons Ltd.

OH)$_2$(H$_2$O)$_{12}$]·8Br·2CH$_3$CN·6CH$_3$OH (**16-{Dy$_3$}$_2$**, Figure 13, left). Among the Dy_6 family of compounds, all six Dy^{III} ions are found to coordinate with a neutral H_2O axial ligand only in this structure. Additionally, the two [Dy$_3$(μ_3-O)$_2$(μ_2-O)$_3$] triangles connected via an organic space ligand in an edge-to-edge fashion.[22] Each of the triangular units is connected by two μ_3-OH atoms, two bridging O atoms from the phenolic oxygen of the ligands, and one bridging −OH atom. The vanishing low-temperature χT and a clear S-shape at around 7 kOe of the $M(H)$ plot suggest possible antiferromagnetic interactions and a toroidal magnetic moment in each triangle (Figure 13, right). A nonmagnetic ground state found for each of the {Dy$_3$} units in this complex is similar to the parent **1-Dy$_3$** molecule. *Ab initio* calculations predict that the anisotropic g_z axes in all the Dy centers align in the plane of the triangle leading to the toroidal magnetic moment in the molecule (Figure 13, left). The con-rotating and counter-rotating toroidal moments on the two triangular subunits were not evidently discussed for this molecule as well. We stress here that more detailed studies of **16-{Dy$_3$}$_2$** are essential to ascertain the FT/AFT nature of its ground state.

In 2017, Xu and co-workers reported a new Dy_6 complex, [Dy$_6$L′4(μ_4-O)(NO$_3$)$_4$]·4CH$_3$OH (**17-{Dy$_3$}$_2$**, H$_3$L′ = 2,6-bis((2-hydroxypropylimino)methyl)-4-methylphenol, Figure 14a) using a methyl-modified Schiff-base ligand.[23] This complex possesses a similar μ_4-O-bridged Dy_6 core as the **15-{Dy$_3$}$_2$**, though the coordination geometries and magnetic interactions are marginally different, which results in different SMT behavior. The measured magnetization under a variable field at 1.9 K shows an S- shaped (Figure 14b) curve, and this indicates that the **17-{Dy$_3$}$_2$** molecule is likely to possess a toroidal moment in its ground state with its conventional magnetic moment larger than **15-{Dy$_3$}$_2$**. The orientation of magnetic anisotropy axes calculated by the electrostatic potential model predicts toroidal arrangement of spins; however, detailed *ab initio* calculations are not provided to discuss the con-rotating and counter-rotating toroidal moments on the two Dy_3 triangles to disprove/prove the FT and/or AFT ground state.

■ NON-DY^{III} TRIANGULAR SMTS

Although limited, other than Dy^{III} ions were also found to exhibit toroidal moments, and this is at the moment restricted to Tb^{III} and Ho^{III} ions, both of which have oblate electron density similar to Dy^{III} ions, and there are no examples from lanthanide ions having prolate electron density stabilized as ground state (such as Er^{III} ion). When we have extended our studies on **7-Cr{Dy$_3$}$_2$** to other lanthanide ions such as Tb^{III}, Ho^{III}, and Er^{III} in place of Dy^{III} and examined the magnetic behavior in these complexes and also in other triangular and wheel-shaped complexes, toroidal magnetic moments were detected in some examples.[20,24] These findings are summarized in this section.

Cr{Ln$_3$}$_2$ (Ln = Tb, Ho, and Er). Focusing on the triangular complexes and the effect changing the Dy^{III} ion would have on

https://doi.org/10.1021/acsomega.1c05310
ACS Omega 2021, 6, 32349−32364

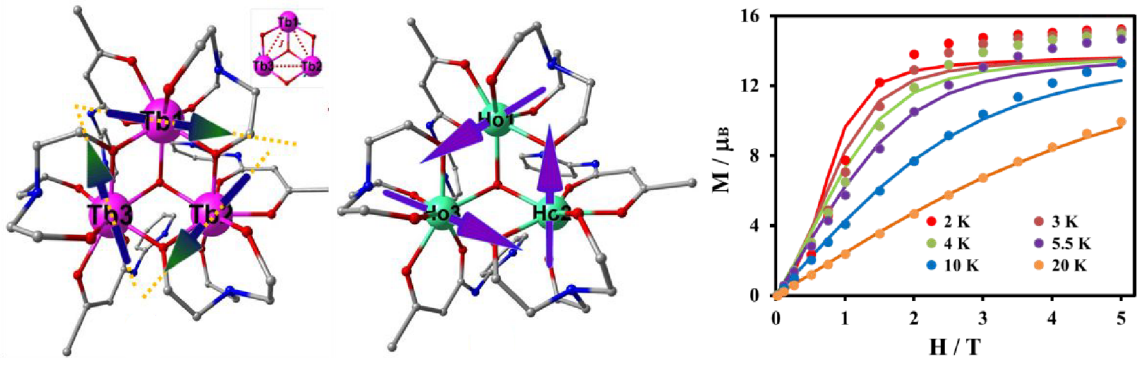

Figure 16. Molecular structure and the orientations of the magnetic anisotropy axes in the ground doublets on the Ln^{III} sites in (left) **5-Tb$_3$**, (middle) **5-Ho$_3$**, and (right) the molar magnetization data for **5-Tb$_3$**. The solid lines are calculated data. Reprinted with permission from ref 20. Copyright 2019, The Royal Society of Chemistry.

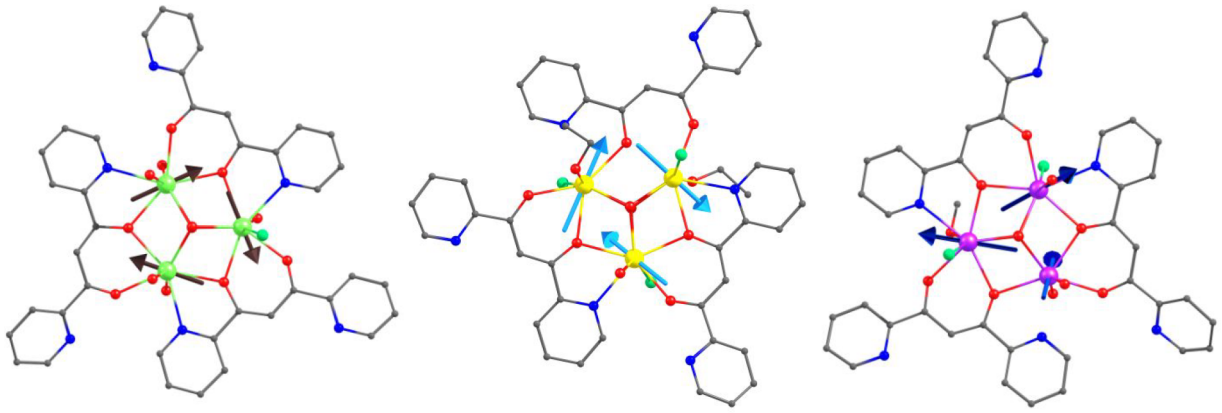

Figure 17. Molecular structure and the orientations of the magnetic anisotropy axes in the ground doublets on the Ln^{III} sites in (left) **6-Ho$_3$**, (middle) **6-Tb$_3$**, and (right) **6-Er$_3$**. Reprinted with permission from ref 28. Copyright 2020, The Royal Society of Chemistry.

the toroidal behavior in the 7-**Cr{Dy$_3$}$_2$** complex, we reported the experimental and theoretical studies on three heptanuclear $[Cr^{III}Ln^{III}_6(OH)_8(o\text{-tol})_{12}(NO_3)\ (MeOH)_5]\cdot 2MeOH$ (Ln = Tb (7-**Cr{Tb$_3$}$_2$**), Ho(7-**Cr{Ho$_3$}$_2$**), and Er(7-**Cr{Er$_3$}$_2$**)) complexes.[24] The S-shaped curves in M vs H at lower T as well as opening up of the hysteresis in single-crystal measurements were absent in these examples. Since both Tb^{III} and Ho^{III} ions are non-Kramers in nature, this encourages stronger tunnelling between the levels and has been suggested to diminish the expected steps in the single-crystal measurements. However, *ab initio* calculations predict toroidal magnetic moments in Tb and Ho analogues but not in the Er analogue (Figure 15). The angle (θ) of magnetic anisotropy axes with the plane of the Ln_3 triangle is in the range of 5.3°−13.9° in 7-**Cr{Tb$_3$}$_2$** and 5.9°−32.4° in 7-**Cr{Ho$_3$}$_2$**. For 7-**Cr{Tb$_3$}$_2$** and 7-**Cr{Ho$_3$}$_2$** complexes, a con-rotating ferrotoroidal ground state is observed due to the presence of the ferromagnetic dipolar coupling between the Ln(III) ions and the presence of S_6 symmetry of the complexes.[24]

As the ground-state electron density of the Tb^{III} and Ho^{III} ions in the ligand field has oblate character and the μ_3-O atom has the largest negative charges, the electrostatic repulsion clearly favors the corresponding g_{zz} axes of the $\{Ln_3\}$ triangle to lie outward in a circular pattern, leading to the presence of toroidal moments. For the 7-**Cr{Er$_3$}$_2$** complex, the Er^{III} ion in the ligand field stabilizes $m_J = \pm 15/2$ as the ground state and therefore has prolate electron density. Hence, the corresponding g_{zz} axis tends to orient perpendicular to the $\{Er_3\}$ triangular plane and results in a nontoroidal arrangement. If the 7-**Cr{Dy$_3$}$_2$**, 7-**Cr{Tb$_3$}$_2$**, and 7-**Cr{Ho$_3$}$_2$** complexes intertriangle dipolar-induced splittings are analyzed, it is clear that ΔE(FT-AFT) is 0.28 cm^{-1}, 0.65 cm^{-1}, and 0.1 cm^{-1}, respectively, with the largest gap detected for the 7-**Cr{Tb$_3$}$_2$** complex rewarding such Ln^{III} ions substitution strategy.

Similarly, Langley et al. have synthesized and magnetically and theoretically characterized the Tb and Ho analogues of **5-Dy$_3$**, viz., $[Ln^{III}_3(OH)(teaH_2)_3(paa)_3]Cl_2$ (Ln = Tb (**5-Tb$_3$**), Ho (**5-Ho$_3$**), Figure 16), to investigate their toroidal nature.[20] Remarkably, M vs H plots show an S-shaped curve at low magnetic fields at 2 K for **5-Tb$_3$** (Figure 16, right), but it was absent for **5-Ho$_3$**. The *ab initio* calculations furthermore support toroidal behavior for both **5-Tb$_3$** and **5-Ho$_3$** triangles (Figure 16). These two molecules belong to mixed moment SMTs due to the presence of uncompensated magnetic moments of 0.9 μ_B and 6.0 μ_B for **5-Tb$_3$** and **5-Ho$_3$**, respectively.[10] For non-Kramer ions, the toroidal behavior is rare; however, the toroidal moments in **5-Tb$_3$** and **5-Ho$_3$** are favored by the oblate nature of Tb^{III} and Ho^{III} ions, allowing the magnetic axes to lie in the plane of the Ln_3 triangles as observed for **5-Dy$_3$**.

Recently, along with the Dy analogue (**6-Dy$_3$**), Caporale et al. have reported another set of Ln_3 triangles, viz., $[Tb_3(\mu_3\text{-}OH)_2(o\text{-}dppd)_3(CH_3CH_2OH)_3Cl_3][Tb_3(\mu_3\text{-}OH)_2(o\text{-}dppd)_3(H_2O)(CH_3CH_2OH)_2Cl_3]Cl_2\cdot H_2O$ (**6-Tb$_3$**), $[Ho_3(OH)_2(o\text{-}dppd)_3Cl(H_2O)_5]Cl_3\cdot 3H_2O$ (**6-Ho$_3$**), and $[Er_3(OH)_2(o\text{-}dppd)_3Cl_2(H_2O)_3(CH_3OH)]Cl_2\cdot 3H_2O\cdot CH_3OH$ (**6-Er$_3$**) and characterized their toroidal behavior (Figure 17).[28]

https://doi.org/10.1021/acsomega.1c05310
ACS Omega 2021, 6, 32349−32364

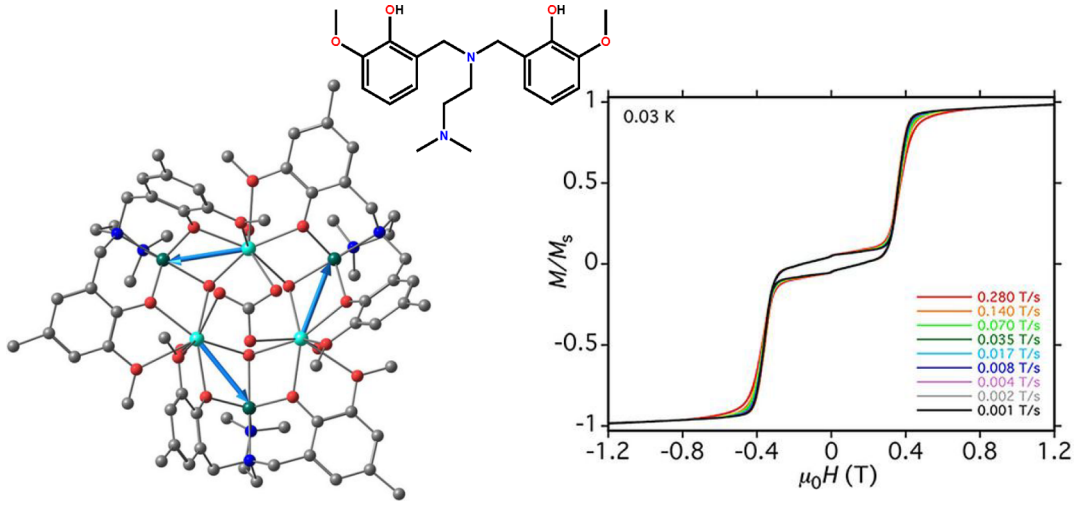

Figure 18. (Left) Molecular structure and the orientations of the magnetic anisotropy axes in the ground doublets on the Dy^{III} sites in **18-Zn_3Dy_3** and (right) magnetization (M) vs field hysteresis loops for a single crystal of **18-Zn_3Dy_3** at 0.03 K and the indicated field sweep rates. Reprinted with permission from ref 30. Copyright 2017, John Wiley & Sons Ltd.

The metal array is the same as seen in **6-Dy_3**. No S-shaped profile at a low-field M vs H plot is observed for these complexes as well. Theoretical calculations predict that the Ho analogue has a toroidal arrangement of spins the same as **6-Dy_3**, but **6-Tb_3** does not support a toroic spin state owing to the changes in the coordination environment. The prolate nature of the Er^{III} centers in **6-Er_3** yields significant transverse anisotropy and hence a strong QTM that leads to the absence of toroidal moments (Figure 17) and suggests that it is hard to witness toroidal moments in Er^{III} ions.

Apart from the complexes discussed here, Chandrasekhar and co-workers have reported a Zn_3Ln_3 SMT,[30] $[Zn_3Ln_3(\mu_6\text{-}CO_3)(\mu_3\text{-}OH)_3(L)_3(H_2O)_3]\cdot 3(ClO_4)\cdot NO_3$ (Ln = Dy (**18-Zn_3Dy_3**), Tb (**18-Zn_3Tb_3**), LH_2 = 6,6′-{[2-(dimethylamino)-ethylazanediyl]bis(methylene)}bis(2-methoxy-4-methylphenol), Figure 18, left), with a μ_6-CO_3^- bridging ligand which bridges all three Ln(III) centers in these molecules. These molecules are formed by the coordination realization of three $[L]^{2-}$, three μ_3-OH^-, and one μ_6-CO_3^- ligands. The metallic core is a Dy_3 triangle surrounded by a Zn_3 triangle. Both nonvanishing low-temperature susceptibility and the S-shaped curve at low-field magnetization plots suggest a magnetic ground doublet state for both **18-Zn_3Dy_3** and **18-Zn_3Tb_3**. Similarly, the first step around the zero field in microSQUID measurements and the loops have an S-shape with a large coercive field opening upon cooling (Figure 18, right), which indicates the presence of toroidal moments. Moreover, *ab initio* calculations predict the orientation of the magnetic moment of the lowest Kramers doublets in **18-Zn_3Dy_3** (Figure 18, left), and Ising doublets in **18-Zn_3Tb_3** are also almost coplanar with the Dy_3 and Tb_3 plane, respectively, which confirms the presence of toroidal behavior in these complexes.[30] As Zn(II) ions are placed on the same plane as that of Dy(III), this tends to polarize the oxygen atom, which in turn coordinates with the Dy(III) ion. This ensures larger negative charges on these oxygen atoms, and therefore the g_{zz} axis points toward the Zn(II) ion. This is also a design strategy to obtain toroidal moments in the Dy_3 motif.

CONCLUSIONS

Though a significant number of molecules with SMT behavior have been reported to be in common, the realization of SMTs is majorly found in Dy_3 systems. In this mini-review, we attempt to give an overview of various structural topologies related to the $\{Ln_3\}$ core that were found to yield SMT properties. Particularly, the peripheral ligands were found to be crucial in dictating the direction of the g_z axis, which in turn strongly correlated to the presence and absence of toroidal moments. The main conclusions observed from this mini-review are summarized below.

(1) ***Multifunctional alcoholic ligands for SMT***: To attain toroidal moments in Dy_3 systems, it is clear that the peripheral ligand design plays an important role. As the anisotropic axis needs to be aligned tangential to the μ_3-O/OH groups, it is important to have ligands that have significantly larger negative charges compared to μ_3-O/OH groups. In this respect, having multifunctional groups such as aldehyde and phenol binding each Dy(III) site in bidentate fashion yield the desired results. Additionally, diamagnetic ions can also be used to enhance the negative charge on the ligand if these ions are placed on the same plane as that of $\{Ln_3\}$.

(2) ***Higher molecule site symmetry key to SMT***: Both the site symmetry of the Dy(III) coordination environment and the overall symmetry of the $\{Dy_3\}$ core were found to help attain toroidal moments. In the $\{Dy_3\}$ family of molecules, the majority of the Dy(III) coordination environment has a C_2 or pseudo C_2 or higher rotational axis passing tangentially to the Dy-μ_3-O/OH vertices, and this helps to reduce the ϕ angle, though the charges on all coordinated atoms and not only the dominant ones play an important role here. Dy_3 SMTs with peripheral ligands containing multifunctional groups such as aldehyde and phenol were found to have a similar type of toroidal magnetic moments, and the tangential angles are similar in examples **1-Dy_3**, **3-Dy_3**, **4-Dy_3**, and **6-Dy_3**. These complexes also have vanishing susceptibility at low T and display an S-shaped curve in the M vs H plot. At the same time, Dy_3 SMTs with amino-polyalcohol ligands such as **2-Dy_3** and **5-Dy_3** lead to mixed moment toroidal examples and therefore remain magnetic at very low temperatures. For this class of SMTs, a finite susceptibility

https://doi.org/10.1021/acsomega.1c05310
ACS Omega 2021, 6, 32349−32364

at low T is typical, and an S-shaped curve in magnetizations was not witnessed in all the examples.

(3) ***Utilizing the $\{Ln_3\}$ motif to enhance SMT in larger clusters***: While several structural motifs beyond $\{Dy_3\}$ to enhance toroidal moments were attempted, many of these polynuclear clusters are made serendipitously, leaving little room for controlling the charges on the peripheral ligands to engineer toroidal moments. On the other hand, enhancing the toroidal magnetic moments by linking two Dy_3 units via 3d ions is found to be a superior strategy compared to linking them via organic ligands. Complexes **7-Cr$\{Dy_3\}_2$**, **7-Cr$\{Tb_3\}_2$**, **7-Cr$\{Ho_3\}_2$**, and **13-$\{Fe_{18}\}$-$\{Dy_3\}_2$** show a fascinating ferrotoroidal behavior, whereas two Dy_3 units connecting via organic ligands **15-$\{Dy_3\}_2$** exhibit antiferrotoroidal behavior due to antiferromagnetic interactions in intratriangles, and in some cases, the toroidal magnetic moments are not maximized (**14-$\{Dy_3\}_2$**).

(4) ***Employing oblate−prolate densities to engineer SMT***: Moreover, recently reported non-Dy SMTs suggest that lanthanide ions with oblate electron densities at their ground state are also suitable candidates for engineering toroidal moments, though the success rate of getting toroidal moments with prolate ions appears to be small. Although more than half-filled ions with oblate electron densities are so far proven to be suitable candidates for engineering toroidal moments, the possibility of such states in other Ln(III) examples cannot be ruled out, and thorough studies covering both experiments and theory are needed to uncover such examples.

AUTHOR INFORMATION

Corresponding Authors

Kuduva R. Vignesh − *Department of Chemistry, Indian Institute of Technology Bombay, Mumbai 400076, India;* orcid.org/0000-0002-0971-2990; Email: krvignesh@chem.iitb.ac.in

Gopalan Rajaraman − *Department of Chemistry, Indian Institute of Technology Bombay, Mumbai 400076, India;* orcid.org/0000-0001-6133-3026; Email: rajaraman@chem.iitb.ac.in

Complete contact information is available at: https://pubs.acs.org/10.1021/acsomega.1c05310

Notes

The authors declare no competing financial interest.

Biographies

Kuduva R. Vignesh completed his Bachelors and Masters degrees in Chemistry at The American College, Madurai, India. He received his PhD under the joint supervision of Prof. G. Rajaraman and Prof. Keith Murray from the IITB-Monash Research Academy, IIT Bombay, Mumbai, India, in November 2016. Then he worked as a postdoctoral researcher under Prof. Kim Dunbar at Texas A&M University, USA, and Prof. Masahiro Ehara at the Institute for Molecular Science, Japan. He is currently working in IIT Bombay as a postdoctoral researcher. His research interest is to design, synthesize, and model mono- and polynuclear transition metal, mixed 3d−4f and lanthanide complexes to understand their various magnetic behavior.

Gopalan Rajaraman (born in Thanjavur, India), after completing his Masters from Bharathidasan University, Trichy, India, moved to the University of Manchester for his PhD. Under the supervision of Prof. R. E. P. Winpenny and Dr E. J. L. McInnes, in 2004, he obtained the PhD. He then undertook postdoctoral stays at the University of Heidelberg, Germany (2005−2007), in the group of Prof. P. Comba and the University of Florence, Italy, in the group of Prof. D. Gatteschi (2007−2009). He joined IIT Bombay, India, as an assistant professor in the latter half of 2009 and became a professor in 2018. His research focuses on employing electronic structure methods to understand the structure, properties, and reactivity of molecules possessing unpaired electrons (open-shell systems). In addition to modeling molecular magnets and their synthesis, his group is also actively involved in the area of modeling biomimic reactions catalysed by high-valent metal-oxo/imido complexes.

ACKNOWLEDGMENTS

We thank the DST and SERB (CRG/2018/00430; DST/CSA-03/2018-10; SB/SJF/2019-20/12) for funding.

REFERENCES

(1) Tang, J.; Hewitt, I.; Madhu, N. T.; Chastanet, G.; Wernsdorfer, W.; Anson, C. E.; Benelli, C.; Sessoli, R.; Powell, A. K. Dysprosium triangles showing single-molecule magnet behavior of thermally excited spin states. *Angew. Chem., Int. Ed.* **2006**, *45*, 1729−1733.

(2) Chibotaru, L. F.; Ungur, L.; Soncini, A. The origin of nonmagnetic Kramers doublets in the ground state of dysprosium triangles: evidence for a toroidal magnetic moment. *Angew. Chem., Int. Ed.* **2008**, *47*, 4126−4129.

(3) Soncini, A.; Chibotaru, L. F. Toroidal magnetic states in molecular wheels: interplay between isotropic exchange interactions and local magnetic anisotropy. *Phys. Rev. B: Condens. Matter Mater. Phys.* **2008**, *77*, 220406.

(4) Luzon, J.; Bernot, K.; Hewitt, I. J.; Anson, C. E.; Powell, A. K.; Sessoli, R. Spin chirality in a molecular dysprosium triangle: the archetype of the non-collinear Ising model. *Phys. Rev. Lett.* **2008**, *100*, 247205.

(5) Ungur, L.; Van den Heuvel, W.; Chibotaru, L. F. Ab initio investigation of the non-collinear magnetic structure and the lowest magnetic excitations in dysprosium triangles. *New J. Chem.* **2009**, *33*, 1224−1230.
(6) Hewitt, I. J.; Tang, J.; Madhu, N. T.; Anson, C. E.; Lan, Y.; Luzon, J.; Etienne, M.; Sessoli, R.; Powell, A. K. Coupling Dy_3 triangles enhances their slow magnetic relaxation. *Angew. Chem., Int. Ed.* **2010**, *49*, 6352−6356.
(7) Lin, S.-Y.; Wernsdorfer, W.; Ungur, L.; Powell, A. K.; Guo, Y.-N.; Tang, J.; Zhao, L.; Chibotaru, L. F.; Zhang, H.-J. Coupling Dy_3 triangles to maximise the toroidal moment. *Angew. Chem., Int. Ed.* **2012**, *51*, 12767−12771.
(8) Novitchi, G.; Pilet, G.; Ungur, L.; Moshchalkov, V. V.; Wernsdorfer, W.; Chibotaru, L. F.; Luneau, D.; Powell, A. K. Heterometallic Cu^{II}/Dy^{III} 1D chiral polymers: chirogenesis and exchange coupling of toroidal moments in trinuclear Dy_3 single molecule magnets. *Chem. Sci.* **2012**, *3*, 1169−1176.
(9) Wang, Y.-X.; Shi, W.; Li, H.; Song, Y.; Fang, L.; Lan, Y.; Powell, A. K.; Wernsdorfer, W.; Ungur, L.; Chibotaru, L. F.; Shen, M.; Cheng, P. A single-molecule magnet assembly exhibiting a dielectric transition at 470 K. *Chem. Sci.* **2012**, *3*, 3366−3370.
(10) Ungur, L.; Lin, S.-Y.; Tang, J.; Chibotaru, L. F. Single-molecule toroics in Ising-type lanthanide molecular clusters. *Chem. Soc. Rev.* **2014**, *43*, 6894−6905.
(11) Gysler, M.; El Hallak, F.; Ungur, L.; Marx, R.; Hakl, M.; Neugebauer, P.; Rechkemmer, Y.; Lan, Y.; Sheikin, I.; Orlita, M.; Anson, C. E.; Powell, A. K.; Sessoli, R.; Chibotaru, L. F.; van Slageren, J. Multitechnique investigation of Dy_3 implications for coupled lanthanide clusters. *Chem. Sci.* **2016**, *7*, 4347−4354.
(12) Li, X.-L.; Tang, J. Recent developments in single-molecule toroics. *Dalton Trans.* **2019**, *48*, 15358−15370.
(13) Trif, M.; Troiani, F.; Stepanenko, D.; Loss, D. Spin-electric coupling in molecular magnets. *Phys. Rev. Lett.* **2008**, *101*, 217201.
(14) Soncini, A.; Chibotaru, L. F. Molecular spintronics using non-collinear magnetic molecules. *Phys. Rev. B: Condens. Matter Mater. Phys.* **2010**, *81*, 132403.
(15) Kaelberer, T.; Fedotov, V. A.; Papasimakis, N.; Tsai, D. P.; Zheludev, N. I. Toroidal dipolar response in a metamaterial. *Science* **2010**, *330*, 1510−1512.
(16) Gossuin, Y.; Hocq, A.; Vuong, Q. L.; Disch, S.; Hermann, R. P.; Gillis, P. Physico-chemical and NMR relaxometric characterization of gadolinium hydroxide and dysprosium oxide nanoparticles. *Nanotechnology* **2008**, *19*, 475102.
(17) Ungur, L.; Langley, S. K.; Hooper, T. N.; Moubaraki, B.; Brechin, E. K.; Murray, K. S.; Chibotaru, L. F. Net toroidal magnetic moment in the ground state of a $\{Dy_6\}$-triethanolamine ring. *J. Am. Chem. Soc.* **2012**, *134*, 18554−18557.
(18) Guo, P.-H.; Liu, J.-L.; Zhang, Z.-M.; Ungur, L.; Chibotaru, L. F.; Leng, J.-D.; Guo, F.-S.; Tong, M.-L. The first $\{Dy_4\}$ single-molecule magnet with a toroidal magnetic moment in the ground state. *Inorg. Chem.* **2012**, *51*, 1233−1235.
(19) Fernandez Garcia, G.; Guettas, D.; Montigaud, V.; Larini, P.; Sessoli, R.; Totti, F.; Cador, O.; Pilet, G.; Le Guennic, B. A Dy_4 Cubane: A New Member in the Single-Molecule Toroics Family. *Angew. Chem., Int. Ed.* **2018**, *57*, 17089−17093.
(20) Langley, S. K.; Vignesh, K. R.; Gupta, T.; Gartshore, C. J.; Rajaraman, G.; Forsyth, C. M.; Murray, K. S. New examples of triangular terbium(III) and holmium(III) and hexagonal dysprosium(III) single molecule toroics. *Dalton Trans.* **2019**, *48*, 15657−15667.
(21) Zhang, Q.; Baker, M. L.; Li, S.; Sarachik, M. P.; Baldoví, J. J.; Gaita-Ariño, A.; Coronado, E.; Alexandropoulos, D. I.; Stamatatos, T. C. *Nanoscale* **2019**, *11*, 15131−15138.
(22) Li, X.-L.; Wu, J.; Tang, J.; Le Guennic, B.; Shi, W.; Cheng, P. A planar triangular Dy_3+Dy_3 single-molecule magnet with a toroidal magnetic moment. *Chem. Commun.* **2016**, *52*, 9570−9573.
(23) Lin, S.-Y.; Wu, J.; Xu, Z. The effect of additional methyl on the magnetic relaxation and toroidal moment of Dy_6 complex. *RSC Adv.* **2017**, *7*, 47520−47526.
(24) Vignesh, K. R.; Langley, S. K.; Swain, A.; Moubaraki, B.; Damjanović, M.; Wernsdorfer, W.; Rajaraman, G.; Murray, K. S. Slow Magnetic Relaxation and Single-Molecule Toroidal Behaviour in a Family of Heptanuclear $\{Cr^{III}Ln^{III}_6\}$ (Ln = Tb, Ho, Er) Complexes. *Angew. Chem., Int. Ed.* **2018**, *57*, 779−784.
(25) Vignesh, K. R.; Soncini, A.; Langley, S. K.; Wernsdorfer, W.; Murray, K. S.; Rajaraman, G. Ferrotoroidic ground state in a heterometallic $\{Cr^{III}Dy^{III}_6\}$ complex displaying slow magnetic Relaxation. *Nat. Commun.* **2017**, *8*, 1023.
(26) Kaemmerer, H.; Baniodeh, A.; Peng, Y.; Moreno-Pineda, E.; Schulze, M.; Anson, C. E.; Wernsdorfer, W.; Schnack, J.; Powell, A. K. Inorganic Approach to Stabilizing Nanoscale Toroidicity in a tetraicosanuclear $Fe_{18}Dy_6$ Single Molecule Magnet. *J. Am. Chem. Soc.* **2020**, *142*, 14838−14842.
(27) Xue, S.; Chen, X.-H.; Zhao, L.; Guo, Y.-N.; Tang, J. Two Bulky-Decorated Triangular Dysprosium Aggregates Conserving Vortex-Spin Structure. *Inorg. Chem.* **2012**, *51*, 13264−13270.
(28) Caporale, C.; Sobolev, A. N.; Phonsri, W.; Murray, K. S.; Swain, A.; Rajaraman, G.; Ogden, M. I.; Massi, M.; Fuller, R. O. Lanthanoid pyridyl-β-diketonate 'triangles'. New examples of single molecule toroics. *Dalton Trans.* **2020**, *49*, 17421−17432.
(29) Ashtree, J. M.; Borilović, I.; Vignesh, K. R.; Swain, A.; Hamilton, S. H.; Whyatt, Y. L.; Benjamin, S. L.; Phonsri, W.; Forsyth, C. M.; Wernsdorfer, W.; Soncini, A.; Rajaraman, G.; Langley, S. K.; Murray, K. S. Tuning the Ferrotoroidic Coupling and Magnetic Hysteresis in Double-Triangle Complexes $\{Dy_3M^{III}Dy_3\}$ via the M^{III}-linker. *Eur. J. Inorg. Chem.* **2021**, 435−444.
(30) Goura, J.; Colacio, E.; Herrera, J. M.; Suturina, E. A.; Kuprov, I.; Lan, Y.; Wernsdorfer, W.; Chandrasekhar, V. Heterometallic Zn_3Ln_3 Ensembles Containing (μ_6-CO_3) Ligand and Triangular Disposition of Ln^{3+} ions: Analysis of Single-Molecule Toroic (SMT) and Single-Molecule Magnet (SMM) Behavior. *Chem. - Eur. J.* **2017**, *23*, 16621−16636.

https://doi.org/10.1021/acsomega.1c05310
ACS Omega 2021, 6, 32349−32364